# Natural Surface Emissions Dominate Anthropogenic Emissions Contributions to Total Gaseous Mercury at Canadian Rural Sites

Irene Cheng[1], Amanda Cole[1], Leiming Zhang[1], Alexandra Steffen[2]

[1]Measurements and Analysis Research Section, Air Quality Research Division, Science and Technology Branch, Environment and Climate Change Canada, Toronto, M3H 5T4, Canada
[2]Processes Research Section, Air Quality Research Division, Science and Technology Branch, Environment and Climate Change Canada, Toronto, M3H 5T4, Canada

*Correspondence to*: Irene Cheng (irene.cheng@ec.gc.ca)



**Abstract.** The Canadian Air and Precipitation Monitoring Network (CAPMoN) measures total gaseous mercury (TGM) at three rural-remote sites. Long-term TGM, ancillary measurements and the Positive Matrix Factorization (PMF) model were used to assess temporal changes in anthropogenic and natural surface emission (wildfires plus re-emitted Hg) contributions to TGM and examine the emission drivers of the observed TGM trends between 2005 and 2018. TGM showed decreasing trends at all sites; the magnitudes (ng $m^{-3}$ $yr^{-1}$) were -0.050 at Saturna for 2010-2015, -0.026 at Egbert for 2005-2018, and -0.014 at Kejimkujik for 2005-2016. The increasing contributions from natural surface Hg emissions at Saturna (1.64% $yr^{-1}$) and Kejimkujik (1.03% $yr^{-1}$) resulted from declining anthropogenic Hg emissions and increasing oceanic and terrestrial Hg re-emissions. The mean relative contributions of natural surface emissions to annual TGM were 65%, 72.5% and 65% at Saturna, Egbert and Kejimkujik. TGM at Saturna was mainly from the Hg pool (53%), Hg re-emissions (14%), and shipping (10%); at Egbert, from the Hg pool (63%), Hg re-emissions (15%), and crustal/soil dust (9%); and at Kejimkujik, from the Hg pool (71%), regional Hg emissions (10%), and Hg re-emissions (8%). Local combustion contributed a few percent of the annual TGM, while the oceanic Hg evasion contribution was 6.6-9.5% for the two coastal sites. Wildfire impacts on annual TGM were 5.6% at Saturna, 1.3% at Egbert, and 2.1% at Kejimkujik. The Hg pool contributions to TGM were greater in the cold season, whereas wildfire and surface re-emission contributions can be significant in the warm season.

## 1 Introduction

Mercury (Hg) is a global pollutant that is toxic to biota and human health. Atmospheric Hg comprises three dominant inorganic fractions including gaseous elemental Hg (GEM), gaseous oxidized Hg or reactive gaseous Hg (GOM or RGM) and particle-bound Hg (PBM). GEM is the predominant form capable of long-range transport and chemical transformation to divalent Hg(II) compounds, such as GOM and PBM. Hg(II) has an atmospheric lifetime of several days to weeks and therefore tends

to deposit locally or regionally. Through dry and wet deposition, atmospheric Hg enters terrestrial and aquatic environments, where it undergoes conversion to methylmercury (MeHg) compounds. The bioaccumulation of MeHg is known to cause severe neurological and reproductive effects (Hong et al., 2012; Driscoll et al., 2013; Obrist et al., 2018).

Emissions drive atmospheric Hg transport, chemical processing, deposition, and subsequent ecosystem impacts. Hg sources to the atmosphere consists of natural emissions (e.g., biomass burning, volcanic and geothermal releases), anthropogenic emissions (e.g., coal combustion, metal smelting, cement production), and re-emissions from terrestrial and aquatic surfaces. Globally, primary anthropogenic Hg emissions account for approximately 30% of the total atmospheric Hg emissions with the remainder from natural emissions and surface re-emissions. The latest global inventories indicate anthropogenic sources emitted 2200-2500 Mg Hg $yr^{-1}$ (Dastoor et al., 2024 and references therein). 200-500 Mg $yr^{-1}$ are emitted from geothermal and volcanic releases and 300-680 Mg $yr^{-1}$ from wildfires. Terrestrial and aquatic surface re-emissions account for 1000-1700 Mg $yr^{-1}$ and 2800-8300 Mg $yr^{-1}$, respectively (Pirrone et al., 2010; Outridge et al., 2018; Streets et al., 2019; Li et al., 2020; Shah et al., 2021; Feinberg et al., 2022; Sonke et al., 2023; Tang et al., 2025). After accounting for atmospheric deposition, the global atmospheric Hg budget is in the range of 3800-4500 Mg. Natural emissions and surface re-emissions of Hg have large uncertainties because of limited spatial and temporal measurements for constraining emission factors. There are also uncertainties with Hg air-surface exchange models and quantifying the proportion of re-emitted Hg originating from natural and anthropogenic sources (Dastoor et al., 2024).

Source attribution analyses, which study the linkages between emission sources and environmental concentrations, have been conducted using receptor methods and chemical transport models (CTMs). Receptor methods, such as Positive Matrix Factorization (PMF) model, principal components analysis (PCA) and back trajectory analysis, are applied to ambient air measurements at a particular location (Cheng et al., 2015 and references therein), whereas CTMs integrate detailed information on Hg emissions, meteorology, chemistry and deposition to predict ambient Hg concentrations typically over a broader region (Horowitz et al., 2017; Shah et al., 2021; Zhang et al., 2023). Receptor methods have been used to identify sources contributing to GEM, GOM, PBM, total gaseous mercury (TGM) (Mazur et al., 2009; Huang et al., 2010; Eckley et al., 2013; Wang et al., 2013; Cheng et al., 2017; Qin et al., 2020; Custodio et al., 2020), and Hg wet deposition (Keeler et al., 2006; Michael et al., 2016). There are numerous modeling studies on atmospheric Hg with some focusing on an improved Hg emissions budget (Fisher et al., 2012; Zhang et al., 2016, 2023), chemical mechanisms (Shah et al., 2016), vegetation uptake (Zhou et al., 2021), and source apportionment estimates (ECCC, 2016; Fraser et al., 2018; Dastoor et al., 2021, 2022).

Anthropogenic Hg emission sources inferred from receptor methods include coal, wood and oil combustion, cement production, iron and steel production, and vehicular traffic. Receptor methods have also been used to assess the effectiveness of emissions control on ambient Hg concentrations. PMF modeling showed that the closure of coal-fired power plants resulted in significant reductions in Hg source contributions to a nearby monitoring site (Wang et al., 2013). Concentration-weighted trajectory analysis revealed steep declines in Hg source contributions over southeastern Canada and northeastern U.S., which were driven by Hg emission reductions from power plants (Cheng et al., 2017). PCA also showed the diminished point source impact on TGM following the closure of a local base metal smelter in Canada (Eckley et al., 2013). Aside from anthropogenic

Hg sources, source attribution studies have revealed the growing importance of natural Hg emissions (e.g., wildfires, oceanic evasion), chemical processing, and long-range transport.

The objective of this study is to determine the source contributions to TGM at three Canadian Air and Precipitation Monitoring Network (CAPMoN) sites using the PMF model and assess their long-term changes. Sources identified from the PMF model are aggregated into anthropogenic and natural surface emission contributions to examine the changes in their relative proportions over time. The long-term CAPMoN TGM measurements is also used to conduct statistical trends analysis and assess the emission drivers of the long-term trends.

## 2 Methods

### 2.1 TGM measurements and ancillary data

The CAPMoN TGM sites are located in Saturna, British Columbia; Egbert, Ontario; and Kejimkujik National Park, Nova Scotia. Saturna (SAT) is a coastal site in western Canada close to the Pacific Ocean. Egbert (EGB) is an inland site in southeastern Canada. Kejimkujik National Park (KEJ) is a coastal site in eastern Canada close to the Atlantic Ocean. The three sites are in rural-remote locations with minimal influence from large emission sources; thus, TGM concentrations at the sites are regionally representative. Refer to Table 1 for additional site information. TGM at other Canadian sites has been analyzed in previous publications (Temme et al., 2007; Cole et al., 2014; MacSween et al., 2022). The CAPMoN TGM sites were selected for this study to provide an update on current concentrations and patterns. The same set of ancillary measurements are also available at the sites to conduct PMF analysis.

TGM is measured using a Model 2537 Hg vapor analyzer (Tekran Instruments Corporation, Toronto, Ontario, Canada), which employs cold vapor atomic fluorescence spectrometry (CVAFS) to quantify TGM. The analyzer is housed in a shelter at each location with the sampling line extending through the rooftop to the outdoor environment. The approximate height of the air inlet above ground is 6 m. Ambient air is sampled at 1.5 L $min^{-1}$ through a heated PFA line maintained at temperatures at least 10°C above ambient. A Teflon filter at the air inlet and back of the analyzer removes particulate matter from the air stream. TGM, including GEM and GOM, is adsorbed onto dual gold cartridges which alternate between sampling and desorption every 5 min. TGM concentrations are reported in units of ng $m^{-3}$ referenced to STP (0°C, 1 atm). Automated calibrations are performed every 25 h using the analyzer's Hg permeation source, verified annually by manual injections of a known amount of $Hg^0$ to zero air using the Tekran Model 2505 Calibration Unit. The permeation rate derived from manual calibrations is expected to be ± 5% of the analyzer's perm rate. Every 35 samples, the permeation source releases $Hg^0$ into the sampled air to assess recovery.

Site operators and field staff perform instrument checks and maintenance activities including sample filter replacement, lamp voltage adjustments, argon tank replacement, etc. Site audits are conducted annually, including verification of the Hg permeation rate and sample flowrate, leak and sample line checks, and gold cartridge replacement if necessary. The 5-min TGM data are quality controlled by flagging instrument parameters (baseline voltage mean and standard deviation, cartridge

difference, sample volume, etc.) that are outside the normal range of operations. The data reviewer checks field notes, site audit reports and wildfire maps, verifies quality control flags, investigates anomalies and outliers, and computes hourly averages for final reporting.

Ancillary measurements of particulate inorganic ions, $SO_2$, CO, total carbon, and air temperature were obtained from CAPMoN and other monitoring networks (Table S1). Inorganic ions, $SO_2$, and temperature were measured at the sites, whereas regionally representative CO and total carbon measurements were within 40 km of the sites. All data have been quality controlled by their respective networks and are publicly accessible. Hourly data were converted to 24-h averages for input into the PMF model.

## 2.2 PMF model

The USEPA PMF model is a multivariate model for the source apportionment of air pollutants, such as speciated particulate matter, VOC, trace elements, and speciated atmospheric Hg. The principles behind the PMF model are detailed in previous studies and the user's guide (Norris et al., 2014; Brown et al., 2015). The PMF dataset consisted of 12 variables including 24-h chemical species concentrations and mean air temperature (Table S1). Each site has 8-14 years of measurements. The long-term data coverage and high-temporal data resolution are sufficient for PMF modeling to capture variations in local and regional sources. Uncertainties were calculated using the equation provided in the user's guide, which is a function of the detection limit (DL) and error fraction (Norris et al., 2014). Based on pollutant tracers, factor profiles were assigned to mercury sources using known source profiles or emissions information from literature. Temperature was included in the model because it is an important driver of wildfire emissions and terrestrial Hg re-emissions (Zhu et al., 2016). The main assumption of the PMF model is that no chemical transformation takes place during atmospheric transport. Thus, we limited the input of reactive or secondary species into PMF. The input of TGM is advantageous over speciated Hg because TGM is the sum of GEM and GOM (oxidized Hg) which tends to be less impacted by chemical reactions.

PMF model runs were performed for each year of data separately resulting in yearly factor profiles. Source profiles can change over time, for example the fuel type and temperature of a forest fire can vary from one fire to another (and is influenced by climate variability); emissions control technology may impact the relative proportions of CO and TGM in the anthropogenic component of the Hg pool; Hg emissions from powerplants and industrial sources have decreased due to domestic regulations. Thus, a constant factor profile assumption over the long-term may not be valid in all cases. Supplement S1 summarizes the comparison between the yearly runs and a single run for the entire time series. Results from the yearly runs are presented in the main paper as they reproduced the daily TGM variability better. We ran the model using 6 factors and attempted additional runs with 5 and 7 factors (sensitivity runs in Supplement S2). The regression fit between modeled and observed TGM and interpretability of the factors among the yearly runs were assessed to determine the optimal number of factors. For the final 6-factor solution, the model-observed $R^2$ values for TGM were $\geq 0.5$ for all yearly runs. Plots of PMF modeled versus observed 24-h TGM are shown in Fig. S1. The plots illustrate strong correlations between modeled and observed TGM at the three sites with $R^2$ of 0.71-0.76. The modeled TGM also reproduced the time-series of the observed TGM quite well except for a few

elevated TGM concentrations at KEJ in early 2005 (residuals analysis in Supplement S3), which suggests that the final 6-factor PMF solution was a good fit to the observations.

There was one factor in the PMF solution that could represent both surface re-emissions and wildfires. To distinguish between the sources, we examined the covariance in the source contributions and regional fire radiative power (FRP) from MODIS data (NASA, 2023). We identified a FRP threshold for screening wildfire-influenced daily source contributions. Source contributions below the FRP threshold were assumed to be from surface re-emissions.

Anthropogenic and natural surface emission contributions were derived from source contributions. Factors representing local or regional combustion and secondary sulfate were classified as anthropogenic. Natural surface emissions include factors representing wildfires, terrestrial surface re-emissions (GEM re-emissions, dust resuspension), and oceanic evasion. The definition of natural surface emissions discussed in this paper does not necessarily refer to the natural origin of the emissions. Hg re-emissions from land and water surfaces originate from both natural and anthropogenic sources; however, their relative contributions remain uncertain. The Hg pool encompasses both natural surface and anthropogenic Hg emissions, mostly from the Northern Hemisphere, which is subject to long range transport. We assumed the natural surface/anthropogenic contribution was proportional to that of global Hg emissions reported in Pirrone et al. (2010) and Streets et al. (2019), which was estimated to be 68.5%/31.5%.

### 2.3 Long-term trends analysis

Long-term trends analyses were performed using the Theil-Sen slope estimator. The analysis was applied to observed daily TGM concentrations and TGM source contributions (absolute and relative). We computed the annual rate of change and those for the cold (Nov to Apr) and warm (May to Oct) seasons separately to assess whether the trends differ. The TGM analysis period is indicated in Table 1; however, some years of data were unavailable for statistical trends analysis. At SAT, the 2016 data did not meet the data completeness threshold (50% of data available for each season) for trends analysis. TGM concentrations were not measured in 2017 at SAT; thus, the trends analysis was not extended to 2018. KEJ was relocated 3 km south of the original site in February 2017, and the TGM analyzer was changed from the Tekran 2537B to 2537X model. Concurrent TGM measurements at KEJ and the new site (KEB) indicate TGM was significantly higher at KEB. The monthly mean hourly TGM absolute and relative differences were 0.2-0.29 ng $m^{-3}$ and 16.6-21.5%. The cause of the difference may have been the change in instrument model but this is inconclusive and therefore, the 2017-2018 data at the new site were excluded from the long-term trends analysis. Details on the model B and X measurement intercomparison are discussed in Supplement S4.

**Table 1: CAPMoN TGM site information**

| Site ID (site name, province) | Latitude, longitude | Time zone (UTC offset) | Site characteristics | Period of data analyzed |
|---|---|---|---|---|

| | | | | |
|---|---|---|---|---|
| SAT (Saturna, British Columbia) | 48.775, -123.128 | PST (UTC-8) | Coastal site near the Pacific Ocean | 2009-2018 (no data collected in 2017) |
| EGB (Egbert, Ontario) | 44.231, -79.783 | EST (UTC-5) | Inland site in southeastern Canada, agricultural activities nearby | 2005-2018 |
| KEJ (Kejimkujik National Park, Nova Scotia) | 44.432, -65.203 | AST (UTC-4) | Coastal site near the Atlantic Ocean, forested area nearby | 2005-2016 |

165

## 3 Results

### 3.1 Saturna

#### 3.1.1 Overview of TGM concentrations

The range in annual mean TGM concentrations were 1.14-1.49 ng $m^{-3}$ at Saturna (SAT) during 2009-2018. Annual descriptive
170 statistics are summarized in Supplement Table S2. The variability in 24-h TGM was assessed using relative standard deviation (RSD). The RSD was 9.7% and decreased over time. The $75^{th}$ percentile concentrations varied between 1.22 and 1.61 ng $m^{-3}$ depending on the year (Fig. 1). Mean TGM was highest in the spring (Mar - May) and lowest in the fall (Sep - Nov); the means were comparable for the winter (Dec - Feb) and summer (Jun – Aug). The seasonal pattern at SAT was consistent with those reported for other Canadian and northern hemisphere rural-remote sites (Cole et al., 2014; ECCC, 2016). Diel patterns in TGM
175 differed between seasons. The diel amplitude was 4% for winter, 6% for spring, 14% for summer, and 4% for fall. In addition to the strong diel cycle in the summer, TGM also peaked earlier (7:00-8:00 PST) than in other seasons. Spring and fall peaks in hourly TGM were broader typically occurring during 8:00-11:00 PST, whereas the hourly TGM peak occurred during 12:00-13:00 LST in the winter. Lower TGM was typically observed during the evening and nighttime. During the 2009-2018 period, the highest and lowest annual TGM were observed in 2010 (1.49 ng $m^{-3}$) and 2015 (1.14 ng $m^{-3}$), respectively (Fig. 1). Annual
180 TGM decreased from 2009 to 2015 and then returned to higher concentrations in 2016 and 2018.

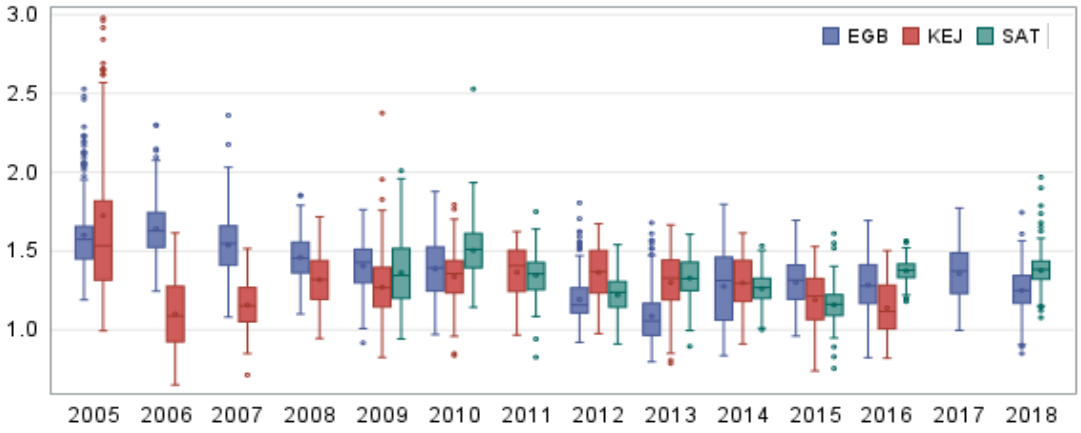


**Figure 1: Box-whisker plots of 24-h average TGM concentrations at Egbert (EGB), Kejimkujik National Park (KEJ) and Saturna (SAT)**

### 3.1.2 PMF factor profiles

PMF model runs were undertaken separately for each year, as well as for the entire 2010-2018 period. For SAT, six factors were generated for each year. Based on the analysis of key variables, the factors represented aged sea-salt aerosols (SSA), fresh SSA, local combustion, the Hg pool, secondary sulfate, and terrestrial GEM re-emissions/biomass burning (BB). The mean percentage of the total factors investigated are shown in Fig. 2 and reported below.

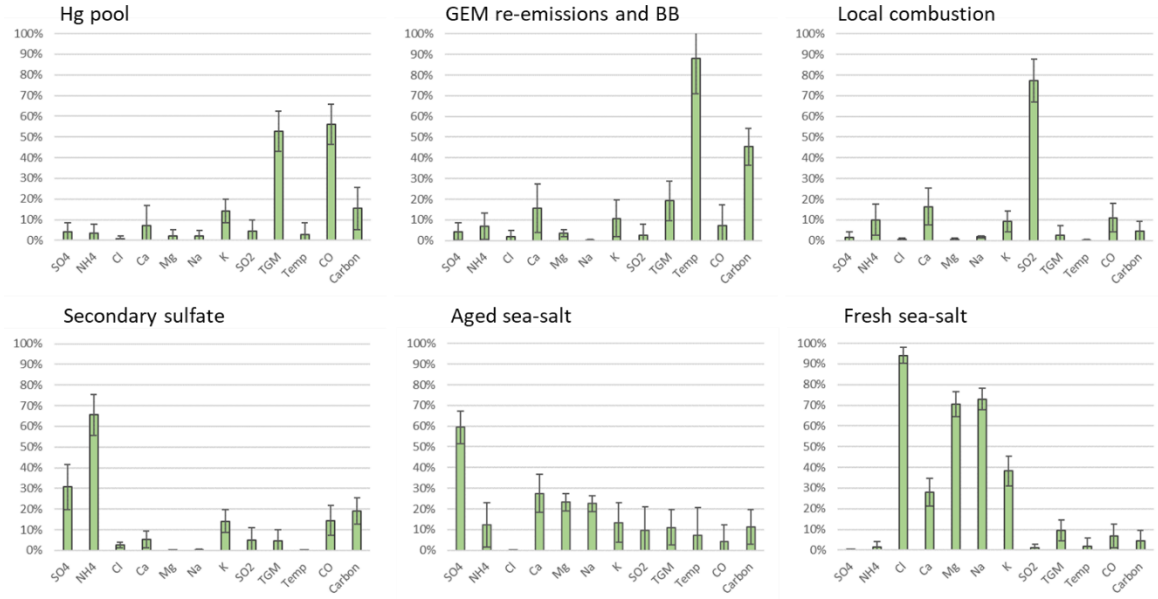

**Figure 2: PMF mean factor profiles for SAT. Error bars indicate standard deviation among the years.**

The aged SSA factor was characterized by moderate abundance of $Ca^{2+}$, $Mg^{2+}$ and $Na^{+}$, elevated $SO_4^{2-}$, and negligible $Cl^{-}$ (Fig. 2), which is a result of the chemical reaction between fresh SSA and acidic compounds. In contrast, the fresh SSA factor had high abundance of $Na^{+}$ and $Cl^{-}$ and negligible $SO_4^{2-}$. The TGM percentage in the aged and fresh SSA factors were ~10% each. $Na^{+}$ and $Cl^{-}$ represent a potential marine source of Hg, such as oceanic Hg evasion or shipping emissions. The combustion factor was characterized by high abundance of $SO_2$ (77%). $SO_2$ is a short-lived pollutant (lifetime of a few days) and is emitted in large quantities from combustion sources, especially coal combustion and metal smelting which are also important anthropogenic Hg sources. The TGM percentage in the combustion factor was only 3%. The Hg pool was identified based on the high abundance of CO (56%). The Hg pool consists of natural, anthropogenic, and re-emitted Hg mostly from the Northern Hemisphere that is subject to long range transport (Selin and Jacob, 2008). CO is emitted from fossil fuel combustion and wildfires. It has a longer lifetime in the order of a few months compared with $SO_2$, which allows for it to be transported long distances by advection (Jeffery et al., 2024) and accumulate in the hemispheric background. This characteristic is similar to that of GEM and TGM. The TGM abundance was the highest in this factor (53%). The secondary sulfate factor had moderate abundance of $SO_4^{2-}$ and high abundance of $NH_4^{+}$; these chemical species were likely produced via the reaction between gaseous ammonia and acidic gases. The TGM percentage in the sulfate factor was 5%. The last factor was representative of GEM re-emissions/BB, identified by the relatively higher temperature in this factor (88%) and presence of total carbon (45%), and $K^{+}$ (11%). The TGM percentage in this factor was 10%. Warm temperatures are conducive to the production of wildfires and GEM volatilization from land and water surfaces. Total carbon and $K^{+}$ are also typically emitted from wildfires. The $K^{+}$ percentage for re-emissions/BB factor was comparable to those in other factors. This may be because this factor is only partially due to wildfires, and re-emissions of GEM would not be associated with $K^{+}$. As well, $K^{+}$ can also be released from the continental crust, soil and vegetation (Zhang et al., 2008) and is very common in pollen (Lee et al., 1996). Since SAT is a coastal site, the source of $K^{+}$ may include SSA. Potassium is also associated with coal combustion (Yu et al., 2018), although this is less likely the case for the rural-remote sites in this study.

### 3.1.3 Overview of TGM source contributions

The mean relative contribution to annual TGM for the 2010-2018 period at SAT was 65.0% from natural surfaces with the remainder from anthropogenic emissions. This corresponds to mean annual TGM contributions of 0.85 ng $m^{-3}$ and 0.46 ng $m^{-3}$, respectively. These results are consistent with the PMF run performed for the entire time series, showing natural surface emission contributions to TGM exceeded anthropogenic contributions (Supplement S1). The breakdown of TGM source contributions (concentrations and percentage basis) are shown in Fig. 3. TGM was apportioned to the Hg pool (52.9%), terrestrial GEM re-emissions (13.7%), shipping emissions and SSA processing (10%), and oceanic evasion (9.5%). Wildfires (5.6%), secondary sulfate (4.6%), and local combustion (3.8%) contributed a smaller fraction of the annual TGM. Shipping emissions in the Ports of Vancouver and Victoria and along the Strait of Georgia had been a significant source of $SO_2$ and

$PM_{2.5}$ because of the high sulfur content in marine fuels prior to regulations taking into effect in 2012 (Anastasopolos et al., 2021). Marine fuels also contain heavy metals, such as V, Ni and Hg. As $SO_2$ is transported downwind and undergoes chemical transformation, acidic gases react with fresh SSA in the MBL resulting in the formation of aged or processed SSA. The assignment of shipping emissions to SSA processing, instead of local combustion, is discussed further in section 3.1.4. Oceanic evasion of GEM was inferred from the fresh SSA factor, since both GEM and SSA are emitted from the ocean surface. Supplement Figure S2 illustrates the Hg pool contributed a larger TGM percentage in the cold season than warm season (65 % vs. 44 %). In contrast, GEM re-emissions, wildfires, and shipping emissions and SSA processing contributed larger TGM fractions in the warm season than cold season. The TGM wildfire contribution for the warm season was sixfold greater than that of the cold season. For terrestrial GEM re-emissions, the TGM contribution in the warm season was double that of the cold season.

### 3.1.4 Interannual and daily variability

Interannual variability in the relative contribution of anthropogenic TGM was in the range of 28-48% (Fig. 3). Anthropogenic contributions were highest in the earlier period (2010 and 2012) because of the larger contributions from shipping emissions and SSA processing. In 2013, 2014 and 2018, natural surface contributions dominated because of greater TGM contributions from terrestrial and marine re-emissions. There were also enhanced TGM contributions from wildfires in 2018 (14%), which was corroborated by observed wildfire statistics. In 2018, the total number of fires and area burned in British Columbia were 39% and 3 times, respectively, above the 2010-2018 average (Government B.C., 2024). Wildfire characteristics such as location, area burned, and type of biomass burned, can change year to year and lead to variability in the wildfire Hg emissions. The impact of wildfires and oceanic evasion on SAT also depend on transport patterns and meteorology, which vary interannually.

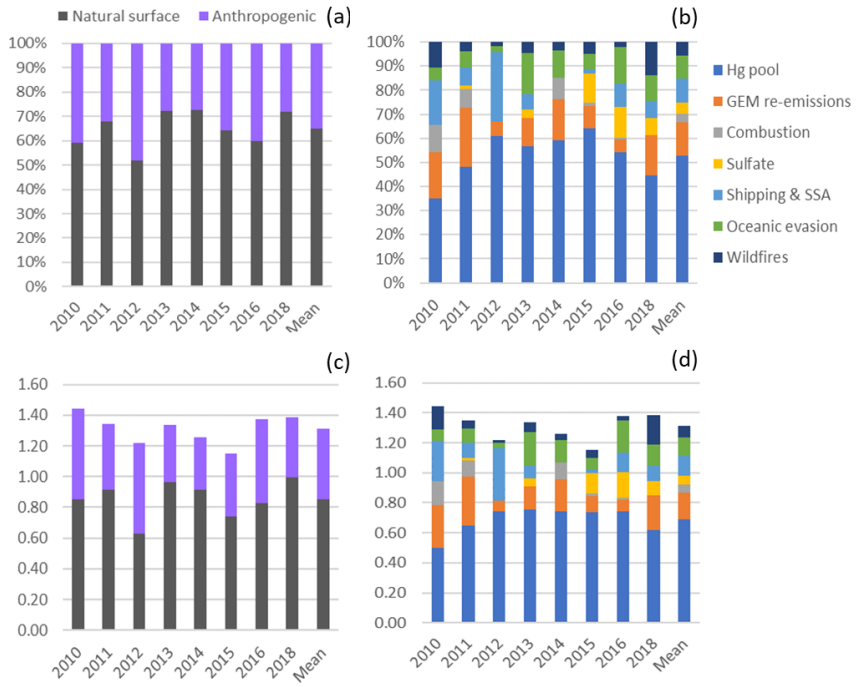


**Figure 3: Impact of natural surface emissions, anthropogenic emissions, and individual emission sources on annual TGM at Saturna (SAT). (a) and (b) plots are relative contributions; (c) and (d) are contributions expressed in concentrations (ng $m^{-3}$). Mean applies to the 2010-2018 period except 2017. Natural surface emissions comprise wildfires, GEM re-emissions, oceanic evasion, and natural surface emissions contributing to the Hg pool. Anthropogenic emissions comprise local combustion, sulfate, shipping and sea-salt processing, and anthropogenic emissions contributing to the Hg pool.**

Figure 4 shows the variation in the daily percentage TGM contributions from natural surface and anthropogenic emissions for SAT and other sites. Relative contributions from natural surface emissions exceeded anthropogenic emissions except on a few occasions. Natural surface emissions contributed 60-100% to daily TGM on most days and were greater during summertime.

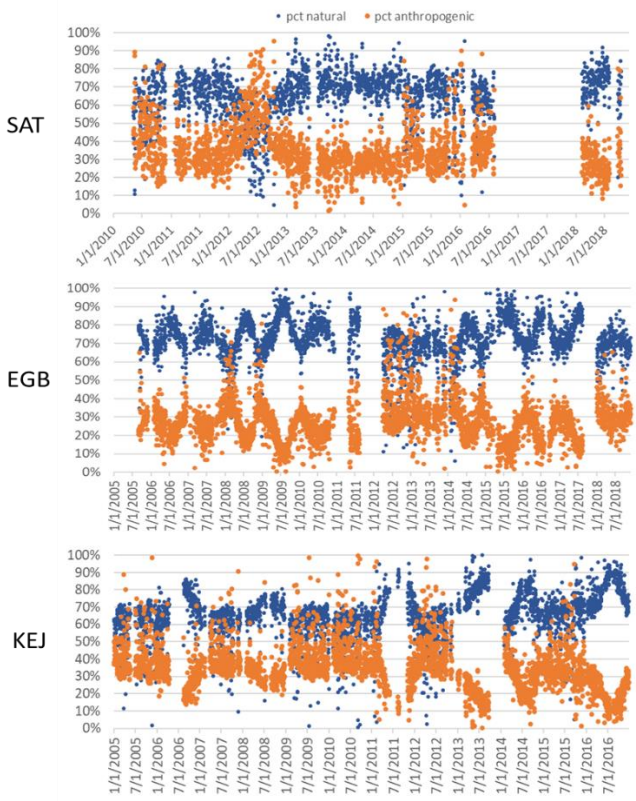


**Figure 4: Relative contributions of natural surface (wildfires plus re-emissions) and anthropogenic emissions to daily TGM at SAT, EGB and KEJ.**

The corresponding plots for individual source contributions at SAT are shown in Fig. 5. There were pronounced seasonal patterns for the Hg pool, terrestrial GEM flux, and wildfire emission contributions. Relative TGM contributions from the Hg pool exhibited a consistent seasonal pattern year over year, exceeding 90% during winter and falling below 30% during summer (Fig. 5). Daily TGM contributions from the Hg pool exceeded 1 ng $m^{-3}$ on a regular basis across the time-series. Those from GEM re-emissions and wildfires were rarely above 1 ng $m^{-3}$. Relative TGM contributions from local combustion, secondary sulfate, and shipping emissions and SSA processing were episodic.

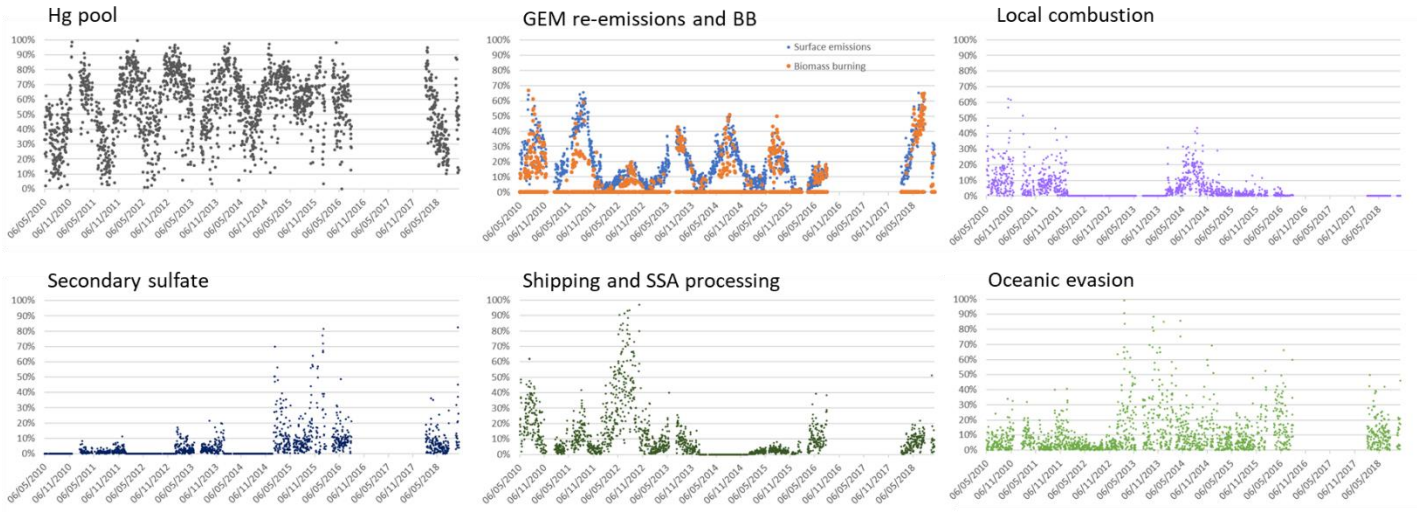


**Figure 5: Relative contributions to 24-h mean TGM from various sources at SAT**

Shipping emissions and SSA processing contributions were noticeably greater than that of oceanic evasion for the earlier period, whereas the case was reversed after 2013. The stronger signature in the earlier period was likely due to higher $SO_2$ concentrations from shipping, resulting in enhancements of acidic compounds in the air to react with fresh SSA. After regulations to limit sulfur content in marine fuels were implemented in 2012, there were substantial decreases in both $SO_2$ and $PM_{2.5}$ concentrations near Canadian port cities (Anastasopolos et al., 2021). According to the Canadian emissions inventory, in addition to $SO_2$ emissions, Hg emissions from marine transportation also decreased from 2010 to 2015 (Fig. S3). This was likely a co-benefit of reducing sulfur in marine fuels. $SO_2$ and Hg emissions in 2015 were 3.6% and 5.4%, respectively, of the 2010 levels. As $SO_2$ emissions from shipping declined, the impact of oceanic Hg evasion became more apparent. The downward trends in Hg and $SO_2$ from shipping emissions and aged SSA production differed from the lack of trends in Hg contributions from local combustion (Fig. 5) and their Hg emission trends, e.g. metals and cement production (Fig. S4). Thus, the shipping factor was distinct from the local combustion factor.

### 3.1.5 Long-term trends

Statistical trends analysis was performed on long-term TGM measurements and PMF modeled TGM source contributions to assess potential causes of TGM trends. Both the observed and PMF modeled TGM showed decreasing trends at SAT with similar magnitudes (-0.0497 ng $m^{-3}$ $yr^{-1}$, $p<0.05$) for the 2010-2015 period (Fig. 6). The comparability in the trends (red line in Fig. 6) and seasonal means (blue line) indicate the PMF model reproduced the TGM observations and adequately captured the seasonal variability over the entire time-series.

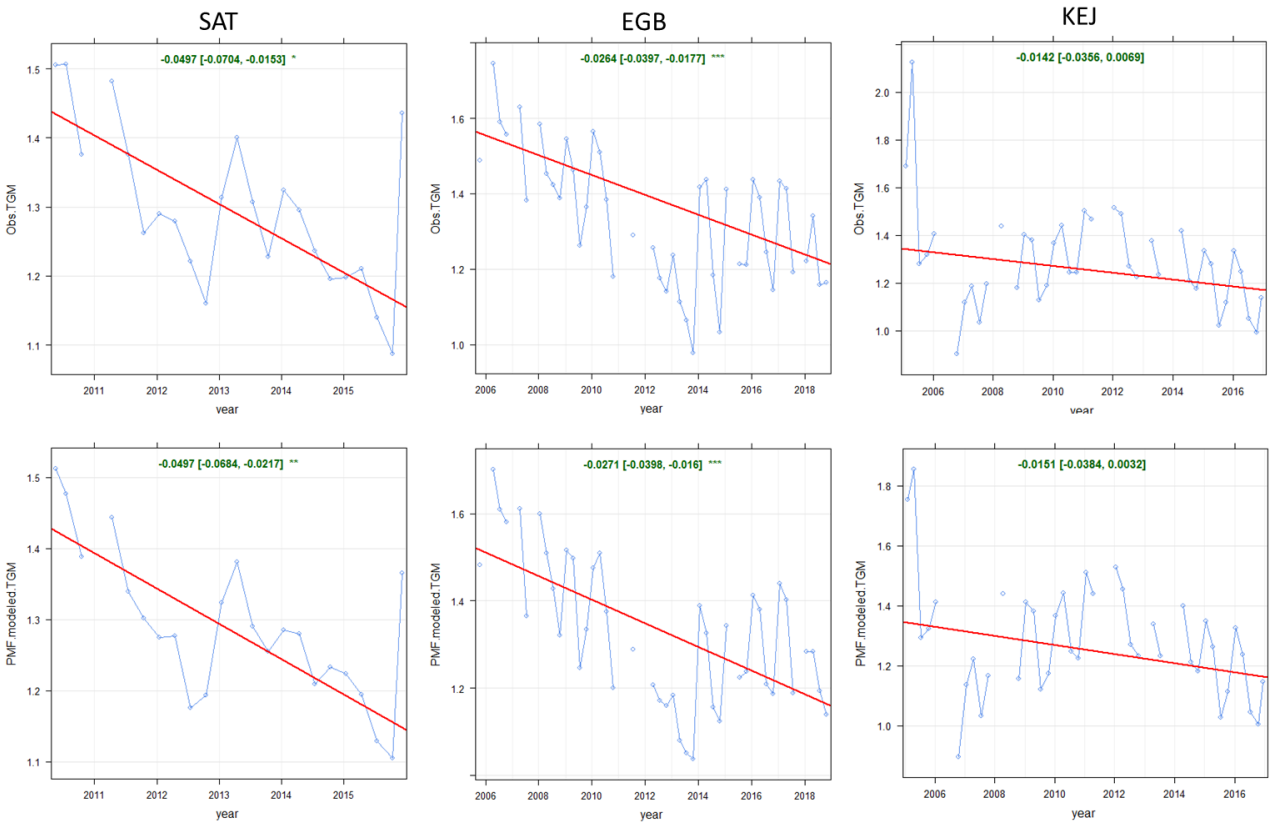


**Figure 6: Long-term trends in observed and PMF modeled TGM concentrations at SAT, EGB and KEJ. Blue line: observed or modeled TGM; red line: trendline; green text: slope of the trendline (ng $m^{-3}$ $yr^{-1}$)**

TGM contributions from the Hg pool showed a slight increasing trend, but it was not statistically significant and opposite in direction of the trends for observed and modeled TGM concentrations (Table 2). TGM contributions from terrestrial GEM re-emissions (-0.0284 ng $m^{-3}$ $yr^{-1}$, $p<0.1$) and shipping and SSA processing (-0.041 ng $m^{-3}$ $yr^{-1}$, $p<0.001$) decreased significantly with time. No statistically significant trend was also found for TGM contributions from local combustion. Within 150 km of SAT, the major combustion sources of Hg were cement manufacturing and primary metal production (Fig. S4). Hg emissions from cement production in British Columbia showed an increasing trend from 2010 to 2015, but the same source type showed a decreasing trend in Washington State. Except for 2010, Hg emissions from metal production were stable. Overall, emissions inventory data support the lack of trend in the TGM contributions from local combustion.

**Table 2: Long-term trends in TGM concentrations and source contributions from the PMF model. SAT: 2010-2015, EGB: 2005-2018, KEJ: 2005-2016. Statistically significant ($p<0.1$) trends are shown in bold.**

| | | Trend | Significance |
|---|---|---|---|

| Site | Parameter/Source | Slope (ng $m^{-3}$ $yr^{-1}$) | Slope (% $yr^{-1}$) | p-value |
|---|---|---|---|---|
| SAT | Obs TGM | **-0.0497** | **-3.46** | 0.010 |
| | Modeled TGM | **-0.0497** | **-3.49** | 0.007 |
| | Hg pool | 0.0453 | 7.70 | 0.154 |
| | Shipping and SSA processing | **-0.0410** | **-21.43** | <0.001 |
| | Terrestrial GEM re-emissions | **-0.0284** | **-13.24** | 0.070 |
| | Local combustion | -0.0125 | -17.26 | 0.212 |
| | Secondary sulfate | 0.0126 | na | 0.102 |
| | Oceanic evasion | 0.0094 | 14.10 | 0.114 |
| | Wildfires | -0.0022 | -6.05 | 0.247 |
| EGB | Obs TGM | **-0.0264** | **-1.69** | <0.001 |
| | Modeled TGM | **-0.0271** | **-1.79** | <0.001 |
| | Hg pool | -0.0171 | -1.76 | 0.140 |
| | Road salt | -0.0012 | -5.21 | 0.142 |
| | Terrestrial GEM re-emissions | -0.0072 | -3.24 | 0.210 |
| | Local combustion | 0.0006 | 0.89 | 0.808 |
| | Secondary sulfate | **-9.69E-8** | **-7.18** | 0.028 |
| | Wildfires | -0.0010 | -6.11 | 0.120 |
| | Crustal/soil | 0.0041 | 4.84 | 0.431 |
| KEJ | Obs TGM | -0.0142 | -1.06 | 0.147 |
| | Modeled TGM | -0.0151 | -1.12 | 0.137 |
| | Hg pool | **-0.0217** | **-2.00** | 0.057 |
| | Regional emission and SSA | **-0.0191** | **-7.62** | <0.001 |
| | Terrestrial GEM re-emissions | **0.0039** | **-37.77** | 0.042 |
| | Local combustion | 0 | 0.00 | 0.576 |
| | Sulfate | 0 | na | 0.876 |
| | Oceanic evasion | 0.0035 | 6.64 | 0.200 |
| | Wildfires | 0.0003 | -24.76 | 0.135 |

Figure 7 shows the trends analysis results for the relative source contributions to annual TGM. The percentage contribution from anthropogenic Hg emissions decreased by 1.64 % $yr^{-1}$ ($p<0.05$) during 2010-2015. The decline was driven by the reduction in the percentage contribution from shipping emissions and SSA processing (-2.92 % $yr^{-1}$, $p<0.001$). In contrast, relative TGM contributions from the Hg pool showed an increasing trend of 4.7 % $yr^{-1}$ ($p<0.05$). The percentage contributions from fresh SSA and secondary sulfate also increased slightly (<1 % $yr^{-1}$, $p<0.1$). Further discussions on cold and warm season trends can be found in Supplement S5.

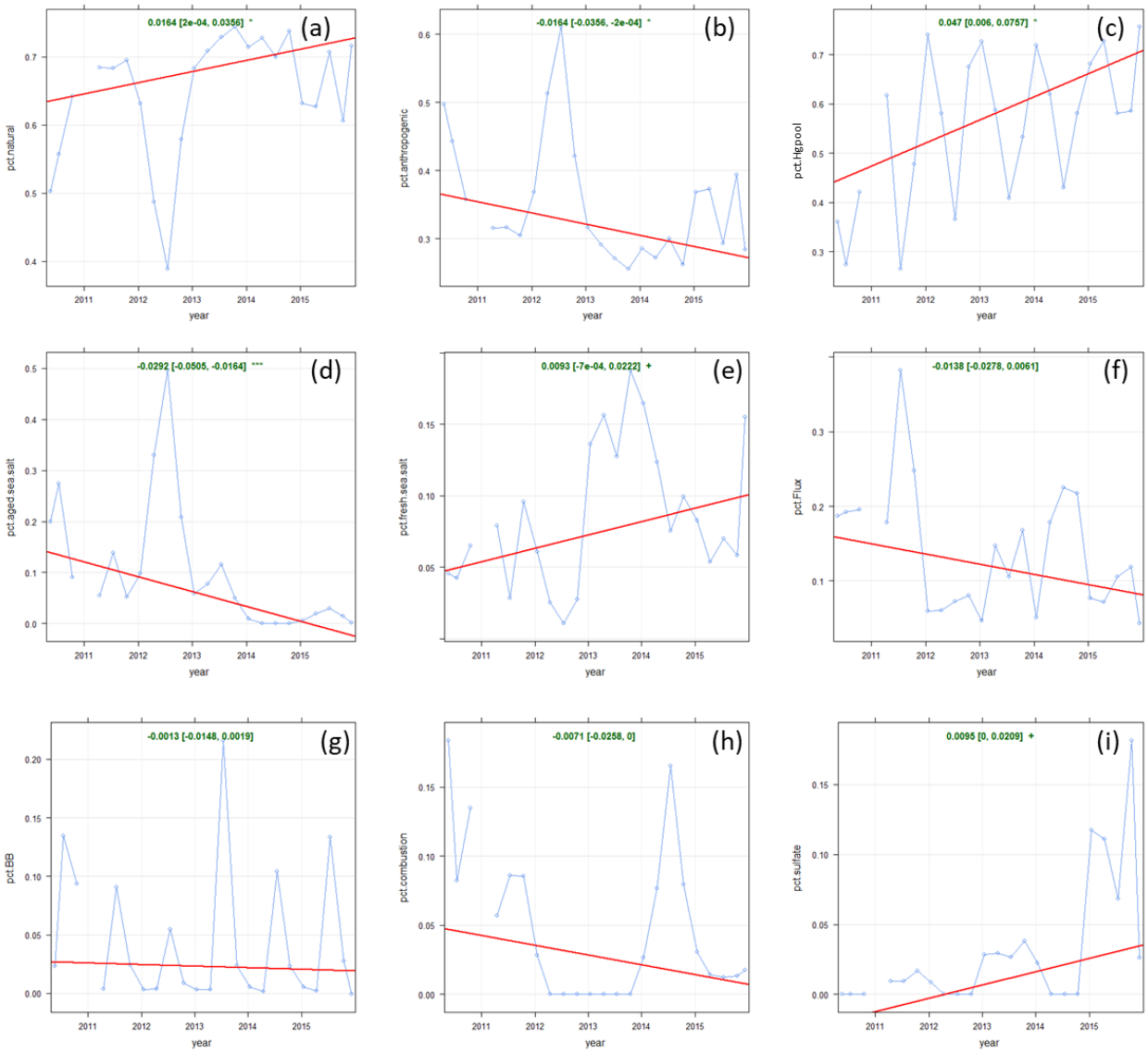


**Figure 7: Long-term trends in relative source contributions at SAT. (a) natural surface emissions (wildfires plus re-emitted Hg), (b) anthropogenic emissions, (c) Hg pool, (d) shipping and SSA processing, (e) oceanic evasion, (f) GEM re-emissions, (g) biomass burning, (h) local combustion, (i) secondary sulfate. Blue line: relative contributions; red line: trendline; green text: slope of the trendline (x100% yr$^{-1}$).**

### 3.2 Egbert

#### 3.2.1 Overview of TGM concentrations

The range in annual mean TGM concentrations was 1.08-1.64 ng m$^{-3}$ at Egbert (EGB) during 2005-2018 (Fig. 1; Table S1). The RSD of 24 h mean TGM was 13.3% and varied from year to year. The 75$^{th}$ percentile concentration ranged between 1.17

and 1.75 ng $m^{-3}$ at EGB depending on the year (Fig. 1). The mean TGM was highest in the winter followed by spring, summer, and fall, respectively. The TGM diel amplitude was 4-5% for winter to summer and 7% in the fall. All seasons showed a broad daytime TGM peak, in which the maximum occurred during 11:00-13:00 LST in winter, summer and fall and during 8:00-10:00 LST in spring. Lower TGM was observed in the evening and nighttime during winter and spring, whereas it was observed at 6:00 LST during summer and fall. For the 2005-2018 period, annual TGM was highest in 2006 and lowest in 2013. There was a sharp decrease in annual TGM from 2005 to 2013 followed by a rebound in 2014 with concentrations remaining stable during 2014-2018 (Fig. 1).

### 3.2.2 PMF factor profiles

Six factors were selected for EGB in the final PMF solution. The factors were assigned to the Hg pool, terrestrial GEM re-emissions and biomass burning (BB), local combustion, secondary sulfate, SSA, and crustal/soil dust (Fig. 8). The Hg pool had the highest abundance of TGM (63%) and CO (60%). Terrestrial GEM re-emissions/BB was characterized by the strong presence of temperature (97%), $K^+$ (34%) and total carbon (43%); the TGM abundance was 17%. The proportions of $SO_2$ and TGM in the local combustion factor were 85% and 6%, respectively. Secondary sulfate was dominated by the presence of sulfate (72%) and ammonium (78%) with a small percentage of TGM (1.8%). The secondary sulfate factor is indicative of regional Hg emissions and chemical transformation including oxidation and gas-particle partitioning. This is because the strong sulfate presence has been associated with regional emissions and oxidation of $SO_2$ from previous source apportionment studies (Liu et al., 2003; Keeler et al., 2006; Gratz and Keeler, 2011; Pancras et al., 2013). Previous back trajectory analyses showed the EGB site was frequently impacted by regional transport (ECCC, 2004; Zhang et al., 2008). A factor was assigned to road salt because of the high abundance of $Na^+$ (79%) and $Cl^-$ (85%), and the relatively greater contributions during the cold season than warm season. The TGM abundance in the road salt factor was 4.1%. Crustal/soil dust was characterized by the high abundance of $Ca^{2+}$ (82%) and $Mg^{2+}$ (77%); the TGM percentage from crustal/soil was 8.7%. In terrestrial ecosystems, Hg is derived either geologically or via atmospheric wet and dry (including litterfall) deposition, and is mainly bound to soil organic matter as oxidized Hg or Hg(II) (Eckley et al., 2016). Hg(II) also has a strong affinity for NaCl particles (Rutter and Schauer, 2007), which may explain the presence of TGM in the road salt factor. Subsequent Hg re-emissions can occur by wind erosion or land disturbance. Soil dust emissions are common around the EGB site because of agricultural areas nearby. Contributions of $Ca^{2+}$ and $Mg^{2+}$ peaked in May and September, which coincide with periods of increased agricultural activity.

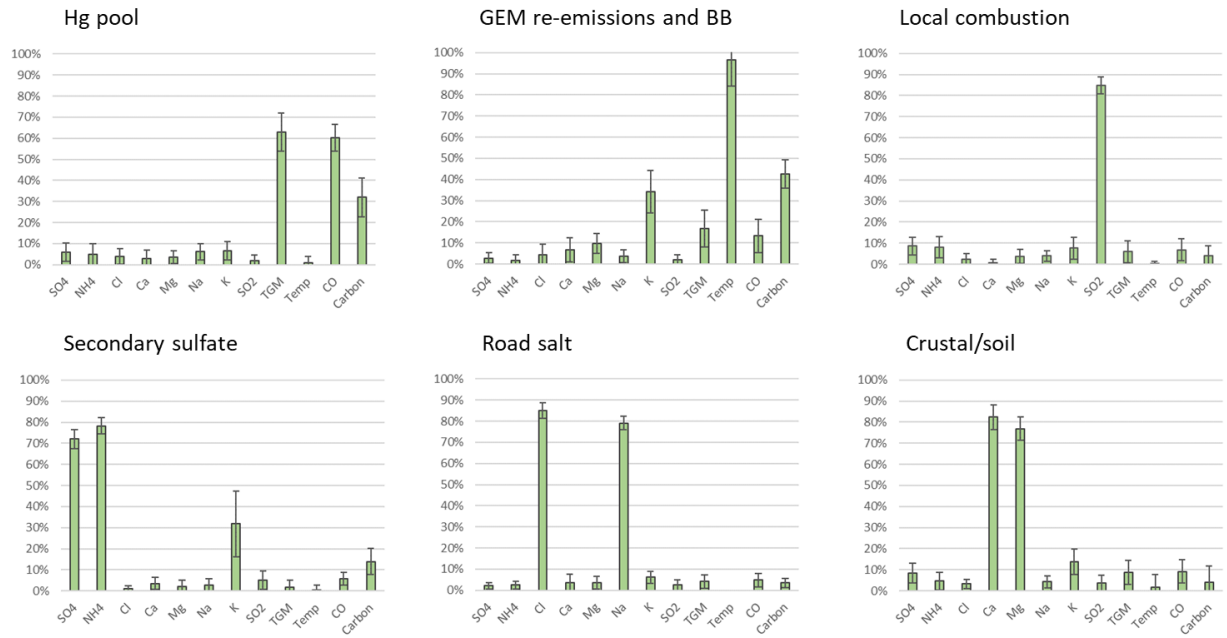


355 **Figure 8: PMF mean factor profiles for EGB. Error bars indicate standard deviation among the years.**

### 3.2.3 Overview of TGM source contributions

The mean relative contribution of anthropogenic emissions to annual TGM was 27.5% at EGB. Natural surface and anthropogenic emissions contributed 0.98 ng $m^{-3}$ and 0.37 ng $m^{-3}$ to the annual mean TGM concentration. The Hg pool (62.9%) contributed the most to annual TGM at EGB followed by terrestrial GEM re-emissions (15.4%), crustal/soil dust (8.7%), local
360 combustion (5.9%), road salt (4.1%), secondary sulfate (1.8%), and wildfires (1.3%), respectively (Fig. 9). Crustal/soil dust and road salt were grouped with GEM re-emissions as they are also re-emitted from the land surface. In this case, the combined contributions from terrestrial surface re-emissions comprised 28.2% of the annual TGM.

The ratios of natural surface to anthropogenic contributions to TGM were 67.8%/32.2% in the cold season and 77%/23% in the warm season (Fig. S5). GEM re-emission contributions comprised 26% of TGM in the warm season compared to only
365 2.8% in the cold season. Crustal/soil TGM contribution in the warm season was twice that of the cold season. In contrast, relative contributions from the Hg pool and road salt were greater in the cold season than warm season.

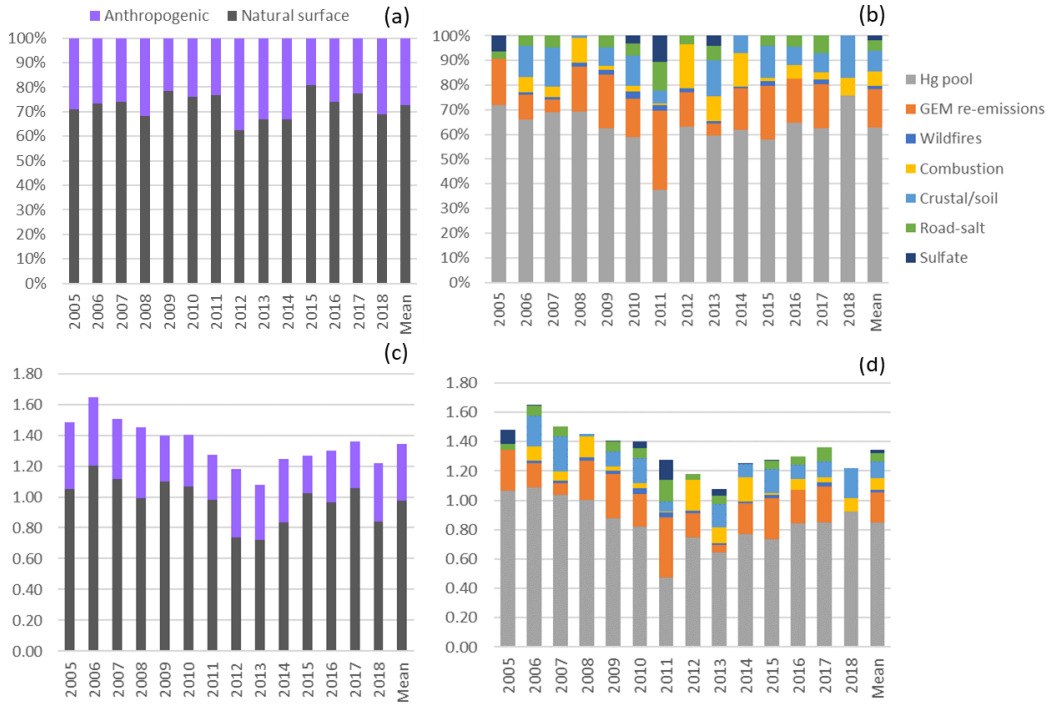


**Figure 9: Impact of natural surface emissions, anthropogenic emissions, and individual emission sources on annual TGM at Egbert (EGB). (a) and (b) plots are relative contributions; (c) and (d) are contributions expressed in concentrations (ng m$^{-3}$). Mean applies to the 2005-2018 period. Natural surface emissions comprise wildfires, GEM re-emissions, crustal/soil dust, road salt, and natural surface emissions contributing to the Hg pool. Anthropogenic emissions comprise local combustion, sulfate, and anthropogenic emissions contributing to the Hg pool.**

### 3.2.4 Interannual and daily variability

During the 2005-2018 period, the annual relative contributions to TGM varied between 19% and 38% for anthropogenic emissions (Fig. 9). Anthropogenic contributions to TGM were especially greater during 2012-2014 because of the higher relative contributions from local combustion. The average relative contribution from local combustion was 6% during 2005-2018; the percentages during 2012-2014 were 10-18%. The annual percentage contribution to TGM during 2005-2018 reached as high as 32% for GEM re-emissions, 18% for local combustion, 17% for crustal/soil dust, 12% for road salt, 11% for secondary sulfate, and 3% for wildfire emissions. The Hg pool contribution was unusually low in 2011 (37.4%) because data were mostly available during the warm season when the background impact tends to be lower. The interannual variability was typically 58-76% in other years.

The warm to cold season ratio varied significantly for TGM contributions from wildfires (10 to 30) and surface emissions (5 to 35). This is because of the year-to-year variability in wildfire emissions. GEM re-emissions depend on meteorology, soil temperature and moisture, land disturbance, canopy shading, etc. which can lead to interannual variability in the emissions. In contrast, the warm to cold season ratios were less variable for the Hg pool contributions (0.5 to 1) and local combustion (0.2 to 1).

Overall, emissions from natural surfaces contributed more to TGM on a daily basis compared to anthropogenic emissions; however, there were some exceptions. Anthropogenic contributions dominated over natural surface contributions in the cold season of 2008, 2012 and 2014 (Fig. 4). While this is expected for the cold season, there were also enhanced anthropogenic daily TGM contributions during the warm season of 2012. There was a pronounced seasonal variation in the Hg pool contributions; the daily percentages were as low as 0.2% in the warm season to as high as 100% in the cold season (Fig. 10). Daily TGM contributions from GEM re-emissions or wildfire can account for more than 50% in the warm season. Daily TGM contributions from local combustion typically comprised less than 30%, though it can occasionally exceed 50%. TGM contributions from crustal/soil and road salt were significant on selected days (up to 90%).

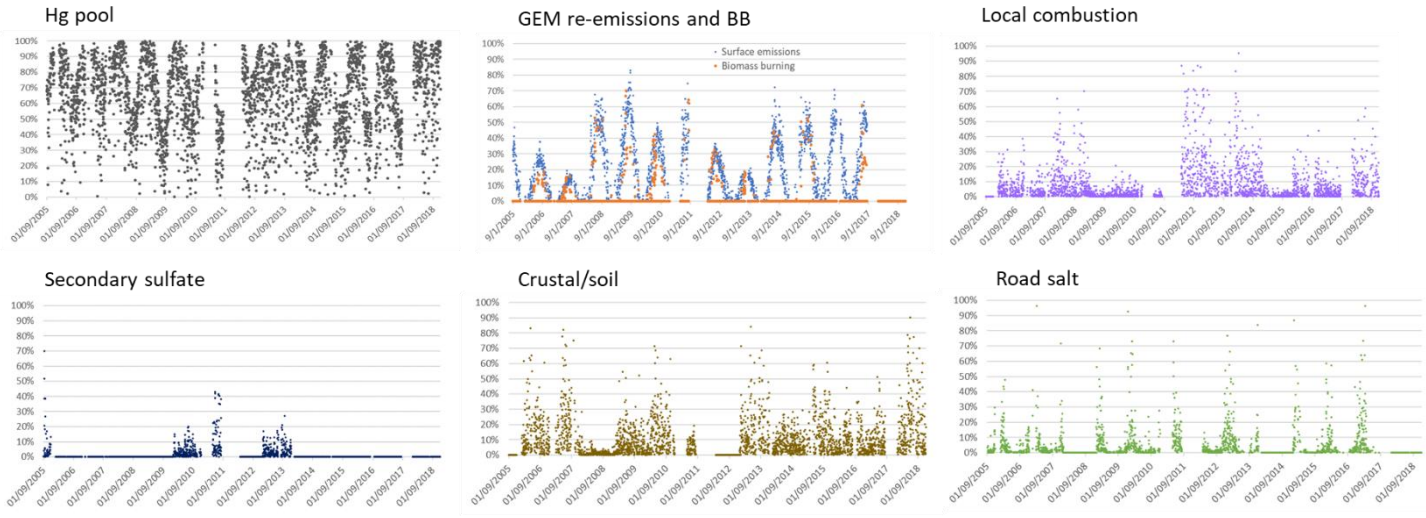


**Figure 10: Relative contributions to 24-h mean TGM from various sources at EGB**

### 3.2.5 Long-term trends

Annual observed TGM at EGB decreased at a rate of -0.026 ng $m^{-3}$ $yr^{-1}$ ($p<0.001$) during 2005-2018. The trend in PMF modeled TGM was similar to the observed trend (-0.027 ng $m^{-3}$ $yr^{-1}$, $p<0.001$; Fig. 6), which indicates good agreement between the PMF model and observations. The observed TGM trend for 2005-2018 was slightly greater than that of 1996-2010 from the previous update (-0.02 ng $m^{-3}$ $yr^{-1}$; Cole et al., 2014). On a long-term scale, the Hg pool was a key driver of the observed TGM trend given the large slope of -0.017 ng $m^{-3}$ $yr^{-1}$ (Table 2). Trends in TGM contributions from other sources were small and not statistically significant. For example, TGM contributions from local combustion showed a flat trend. The major combustion sources near EGB (≤150 km) are iron and steel manufacturing and cement production (Fig. S6). Iron and steel manufacturing Hg emissions had decreased before 2009 and then increased thereafter. Hg emissions from cement production were stable during 2006-2014 and then increased to higher levels after 2014. The change in direction of the emission trends may explain a lack of trend in TGM contributions from local combustion. The trends in relative contributions to TGM from

natural surface and anthropogenic emissions were both non-significant (Fig. 11). This is expected considering the relative source contribution trends were not statistically significant or in some cases the slopes were very small.

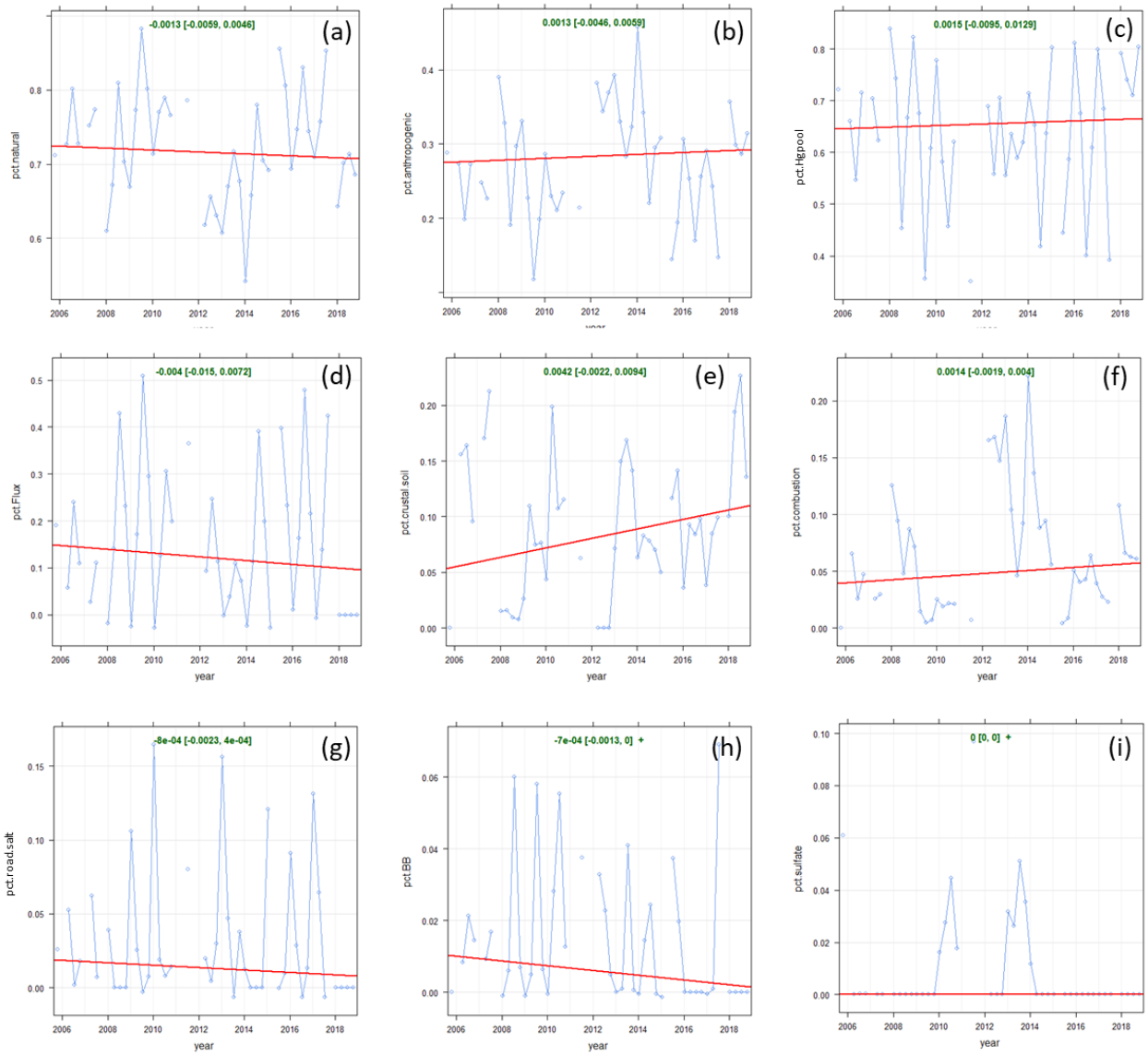


**Figure 11: Long-term trends in relative source contributions at EGB. (a) natural surface emissions (wildfires plus re-emitted Hg), (b) anthropogenic emissions, (c) Hg pool, (d) GEM re-emissions, (e) crustal/soil, (f) local combustion, (g) road salt, (h) wildfires, (i) secondary sulfate. Blue line: relative contributions; red line: trendline; green text: slope of the trendline (x100% $yr^{-1}$).**

Short term patterns in TGM were also observed, e.g. the decrease in TGM concentrations from 2005 to 2013 followed by an increase and then a flat trend. These patterns are likely influenced by local iron and steel manufacturing and cement production (Fig. S6). Hg emissions from electric utilities in the Province of Ontario decreased by 85% between 2005 and 2013 (Fig. S7c) resulting from the phase-out of coal-fired power plants. Reductions in these emissions were also seen in the U.S. Midwest and Northeast regions (Fig. S7g). The pattern in TGM after 2013 was not likely not related to local combustion. This is because while both TGM and $SO_2$ concentrations at EGB decreased during 2005-2013, there was a decoupling of TGM and $SO_2$ after 2013. The rise in TGM was likely from increased contributions from the Hg pool, GEM re-emissions, and crustal/soil Hg (Fig. 9).

## 3.3 Kejimkujik National Park

### 3.3.1 Overview of TGM concentrations

The range in annual mean TGM concentrations was 1.1-1.71 ng $m^{-3}$ at Kejimkujik National Park (KEJ) during 2005-2016 (Fig. 1; Table S2). The RSD of 24 h mean TGM was 12.6% and increased year over year. The 75$^{th}$ percentile concentrations were 1.28-1.82 ng $m^{-3}$ depending on the year. Comparing the statistics over the same period (2009-2016), the mean TGM concentrations among SAT, EGB and KEJ were comparable with no statistically significant differences. The annual TGM across the three CAPMoN sites differed between 3% (in 2014) and 19% (in 2013). The 75$^{th}$ percentile was highest at SAT during 2009-2010, KEJ during 2011-2013, and EGB during 2014-2016, which shows there was no particular site experiencing higher TGM over this period. The seasonal pattern in TGM at KEJ was similar to those of SAT and EGB. Mean TGM was highest during winter and spring and lowest during summer and fall. The diel amplitudes in summer (22%) and fall (14%) were greater than those in winter (5%) and spring (8%). Hourly TGM peaked during 14:00-15:00 LST in the summer and 12:00-14:00 LST in the fall. In the winter and spring, the maximum TGM was typically observed during 11:00-13:00 LST. The TGM minimum occurred during 5:00-6:00 LST in all seasons. For the 2005-2016 period, the highest TGM was observed in 2005 and the lowest in 2006 and 2016. Annual TGM decreased significantly from 2005 to 2006. A parabolic pattern was observed thereafter with concentrations increasing during 2006-2011 and then decreasing during 2012-2016 (Fig. 1).

### 3.3.2 PMF factor profiles

For the KEJ site, the PMF model resolved six factors. The factors represented the Hg pool, terrestrial GEM re-emissions/biomass burning (BB), local combustion, secondary sulfate, aged SSA, and fresh SSA (Fig. 12). TGM (71%) and CO (67%) were the most abundant in the Hg pool factor. GEM re-emissions/BB factor showed a strong presence in temperature (100%) and a weak presence in TGM (10%). Local combustion was characterized by the $SO_2$ abundance (87%); TGM (2%) and CO (2%) were not present in significant amounts. Secondary sulfate showed high abundances for sulfate (64%) and ammonium (77%) with a minor abundance for TGM (1%). Aged SSA was characterized by moderate abundances of $Ca^{2+}$, $Mg^{2+}$, $Na^+$ and $SO_4^{2-}$(22-26% for these ions), and absence of $Cl^-$. Fresh SSA comprised mostly of $Cl^-$ (91%), $Na^+$ (65%) and

$Mg^{2+}$ (60%). The TGM abundances were 10% in aged SSA and 7% in fresh SSA, which were comparable to the SAT coastal site.

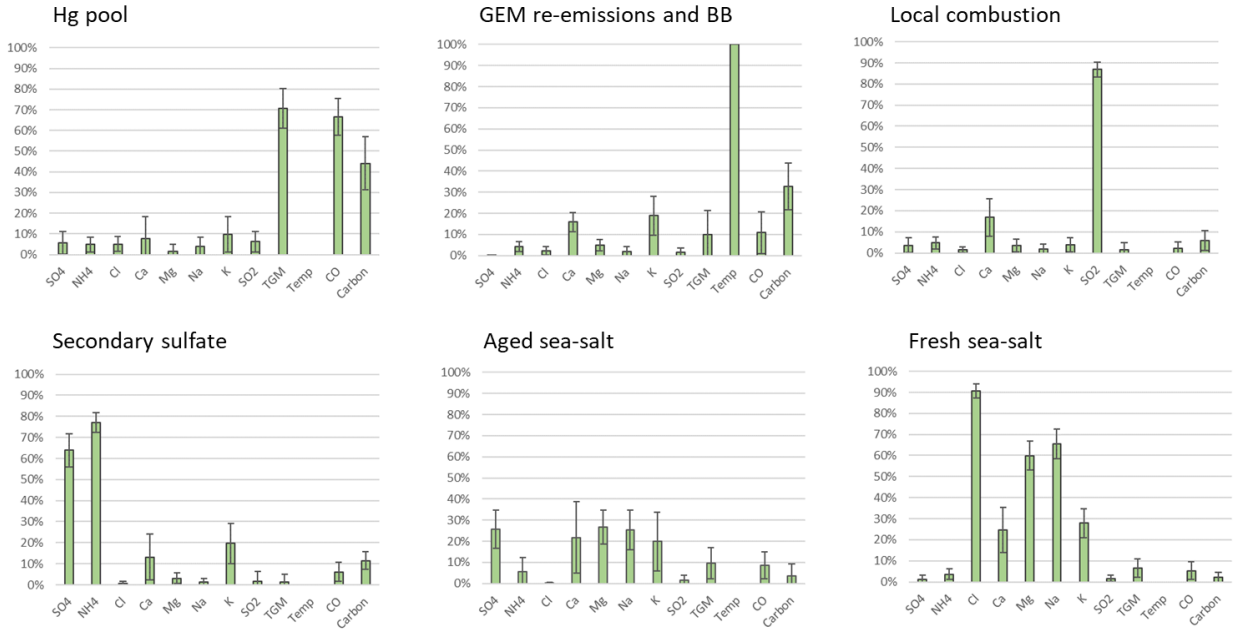


**Figure 12: PMF mean factor profiles for KEJ. Error bars indicate standard deviation among the years.**

### 3.3.3 Overview of TGM source contributions

The mean relative contribution to annual TGM was 65% from natural surface emissions during the 2005-2016 period with the remainder from anthropogenic emissions (Fig. 13). This corresponds to average TGM contributions of 0.83 ng $m^{-3}$ and 0.45 ng $m^{-3}$, respectively. Annual TGM was strongly attributed to the Hg pool (71%), followed by regional emission and SSA processing (9.7%), terrestrial GEM re-emissions (8%), oceanic evasion (6.6%), wildfires (2.1%), local combustion (1.6%), and secondary sulfate (1.4%), respectively (Fig. 13). The regional emission and SSA processing factor is considered anthropogenic origin because aged sea-salt is formed from the reaction of sea-salt and acidic gases ($H_2SO_4$ and $HNO_3$), whose precursors are anthropogenic $SO_2$ and $NO_x$. One of the major sources of $SO_2$ and $NO_x$ is fuel combustion from electric utilities, which are also significant sources of atmospheric Hg. There are no electric utilities within 200 km of KEJ since 2007; however, the site is frequently impacted by air masses from the northeastern U.S. region where there is a high density of electric utilities. Thus, this factor represents both the regional emission contributions of acidic gases and Hg and subsequent chemical processing of fresh SSA as regional air masses are transported across the MBL. On the other hand, fresh SSA is directly emitted

from the ocean and has not been subject to chemical processing. Hg contributions from marine air are mainly from evasion of GEM from the ocean or partitioning of GEM or GOM from sea-salt aerosols.

Emissions from natural surfaces contributed more to TGM in the warm season than the cold season, whereas the case was reversed for anthropogenic contributions to TGM. The proportion of natural surface contributions was 63% in the cold season and 69% in the warm season (Fig. S8). Relative TGM contributions from the Hg pool were greater in the cold season than the warm season. In contrast, GEM re-emissions and wildfire contributions to TGM were greater in the warm season comprising 16% and 5%, respectively, of the warm season TGM.

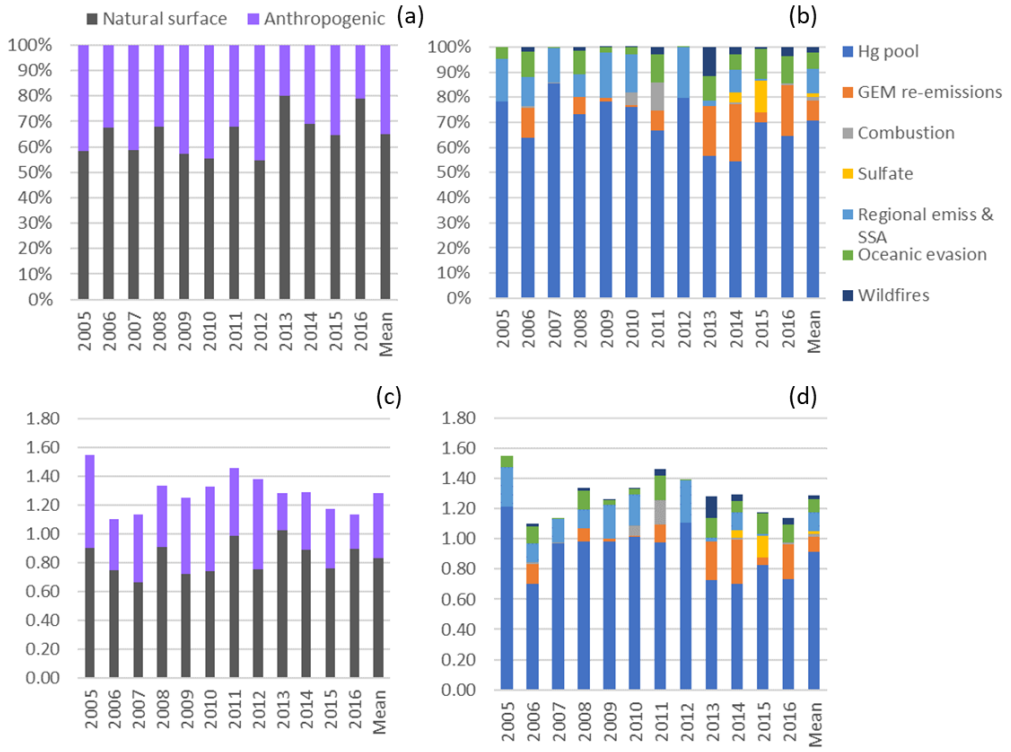


**Figure 13: Impact of natural surface emissions, anthropogenic emissions, and individual emission sources on annual TGM at Kejimkujik (KEJ). (a) and (b) plots are relative contributions; (c) and (d) are contributions expressed in concentrations (ng $m^{-3}$). Mean applies to the 2005-2016 period. Natural surface emissions comprise wildfires, GEM re-emissions, oceanic evasion, and natural surface emissions contributing to the Hg pool. Anthropogenic emissions comprise local combustion, sulfate, regional emissions and sea-salt processing, and anthropogenic emissions contributing to the Hg pool.**

### 3.3.4 Interannual and daily variability

For the 2005-2016 period, relative contributions to annual TGM ranged between 55% and 80% for natural surface emissions (Fig. 13). This percentage was highest in 2013 due to enhanced terrestrial GEM re-emissions and wildfire contributions. The anthropogenic emissions percentage was highest in 2012 because of the greater relative contribution from regional emission and SSA processing. Annual relative contributions from the Hg pool ranged between 55% and 85%. The annual percentage

contribution to TGM during the 2005-2016 period reached as high as 23% for GEM re-emissions, 11% for local combustion, 12.5% for secondary sulfate, 20% for regional emission and SSA processing, 12% for oceanic evasion, and 11.5% for wildfires. Natural surface contributions typically exceeded anthropogenic contributions to daily TGM; however, there were also many days when the latter was equivalent or greater (Fig. 4). Anthropogenic TGM comprised 5-50% occasionally increasing above 70%. The elevated episodes were attributed to regional emission and SSA processing, local combustion, and secondary sulfate. Daily TGM contributions from the Hg pool showed large fluctuations with percentages ranging from 0% to 100%, though they were mostly above 50% (Fig. 14). GEM re-emissions and wildfires contributed upwards of 20% of the daily TGM in the warm season, whereas the contributions were negligible in the cold season. Daily TGM contributions from oceanic evasion were typically below 30% and occasionally reached as high as 90%.

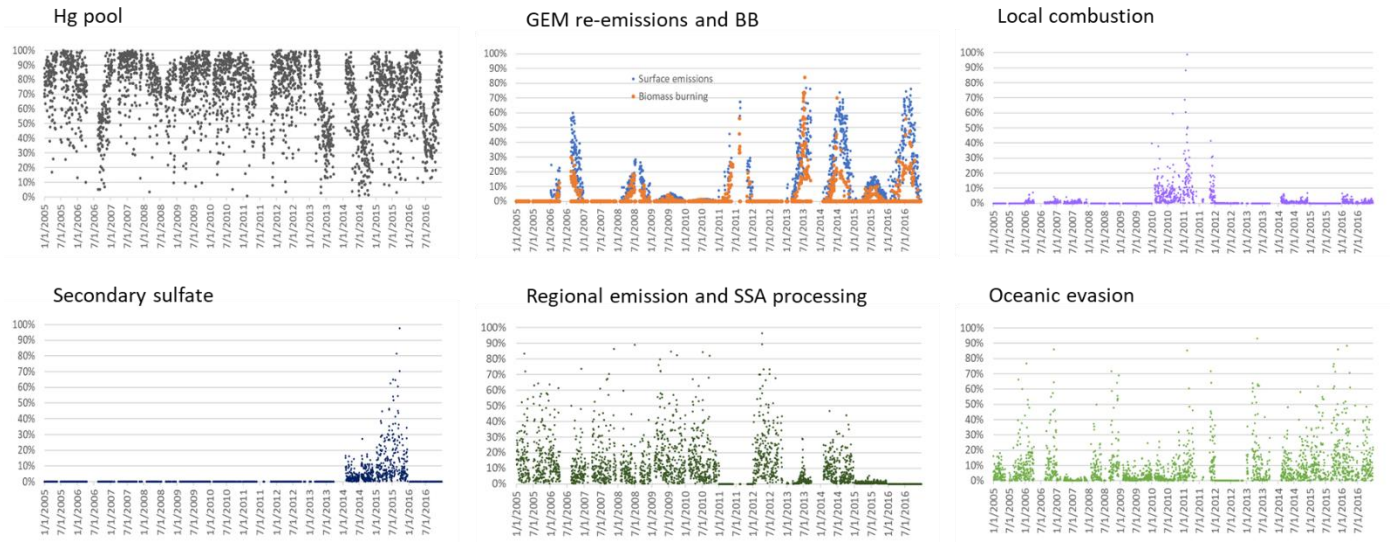


**Figure 14: Relative contributions to 24-h mean TGM from various sources at KEJ**

### 3.3.5 Long-term trends

Figure 6 shows the annual trends in the observed and modeled TGM at KEJ over the 2005-2016 period. The magnitudes of the trend were -0.014 ng $m^{-3}$ $yr^{-1}$ (1.06% $yr^{-1}$) for observed TGM and -0.015 ng $m^{-3}$ $yr^{-1}$ (1.12% $yr^{-1}$) for PMF modeled TGM. Neither trend was statistically significant. The similarity in the trends indicates the PMF model reproduced the variability in observed TGM. The observed TGM trend for 2005-2016 was the same as that of 1996-2010 from the previous update (Cole et al., 2014). Long-term trends in TGM were driven by several sources including the Hg pool, regional emission and SSA processing, and GEM re-emissions. The Hg pool contributions decreased significantly at a rate of -0.022 ng $m^{-3}$ $yr^{-1}$ (Table 2), which outpaced the observed TGM trend. This was also the case for the trend in regional emission and SSA processing contributions (-0.019 ng $m^{-3}$ $yr^{-1}$). These decreasing trends were attenuated by that of GEM re-emissions contributions, which had a slight positive trend of 0.004 ng $m^{-3}$ $yr^{-1}$. The decreasing trend in the TGM contribution from regional emission and SSA

processing was attributed to decreasing Hg and $SO_2$ emissions. On a regional scale, Hg emissions fell from 23.2 Mg $yr^{-1}$ in 2005 to 5.3 Mg $yr^{-1}$ in 2016 corresponding to a 77% reduction (Fig. S7g). In addition, there was also a decrease in ambient $SO_2$ at KEJ (-0.037 µg $m^{-3}$ $yr^{-1}$, $p<0.001$), which was driven by significant $SO_2$ emissions reductions both locally and regionally (Fig. S9). Consequently, SSA processing also decreased with time.

The trend in relative contribution from natural surface emissions showed an increase of 1.03% $yr^{-1}$ ($p<0.001$) for the 2005-2016 period (Fig. 15). This trend is attributable to the steep decline in the percentage contributions from regional emissions and SSA processing (-1.13 % $yr^{-1}$), which is anthropogenic. There were also small percentage increases in natural surface emissions contributions including from terrestrial GEM re-emissions (0.3 % $yr^{-1}$, $p<0.05$) and oceanic evasion (0.33 % $yr^{-1}$, non-sig.). The percentage contribution from the Hg pool showed a decreasing trend of -1% $yr^{-1}$ ($p<0.1$) similar to that in the concentrations.

While long-term TGM concentrations at KEJ are trending downwards, there are shorter term variations that are not captured in the trends analysis. TGM decreased sharply from 2005 to 2006 (Fig. 1), which was consistent with the significant decrease in local Hg emissions from electric utilities (Fig. S10). There was a period of increasing TGM from 2006 to 2011 followed by decreasing TGM from 2011 to 2016. This pattern was consistent with local Hg emissions from oil and gas pipelines and storage emissions. These emissions began to decline in 2011. In fact, no Hg emissions within 150 km of KEJ were reported from 2014 onwards.

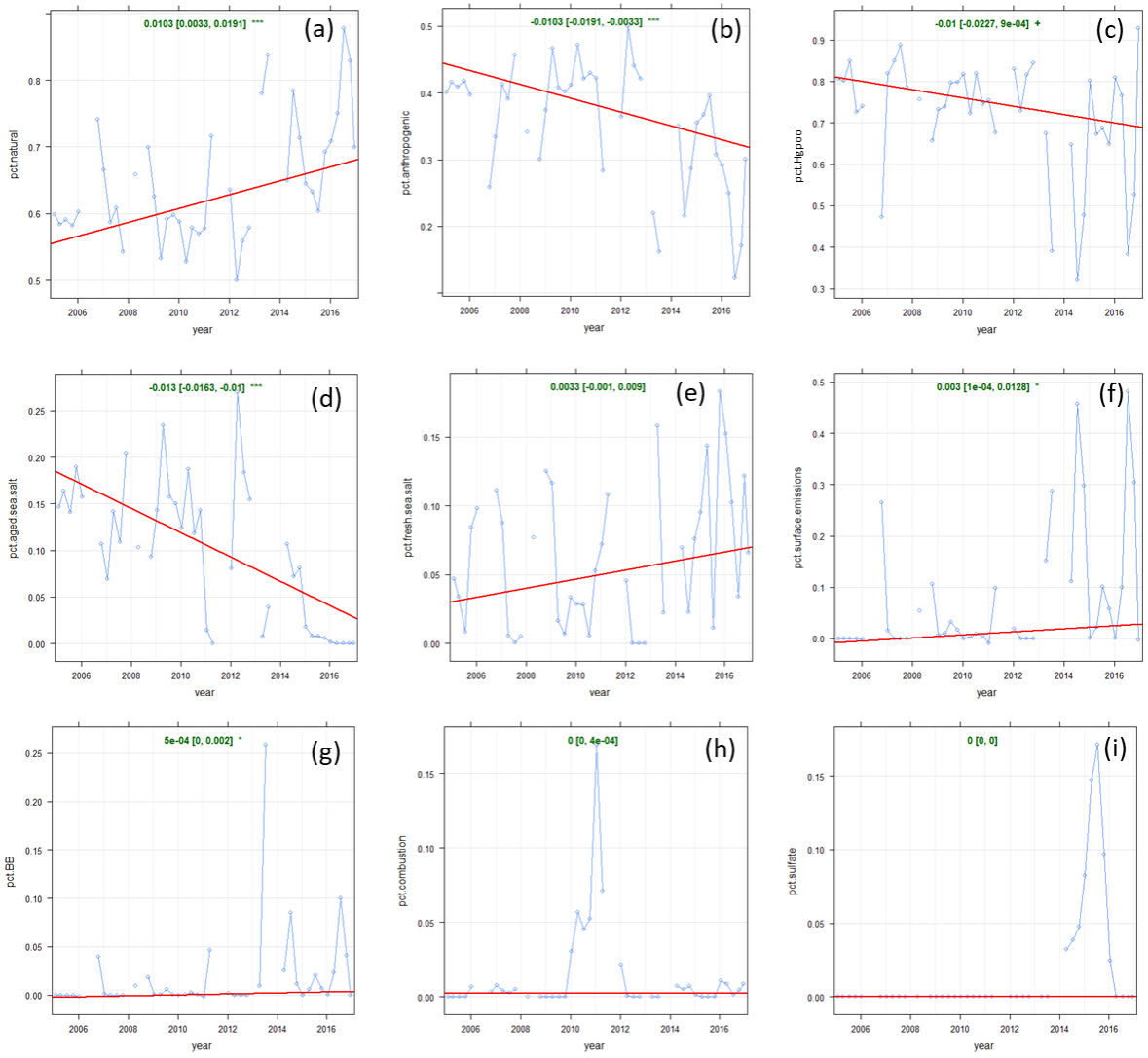


**Figure 15: Long-term trends in relative source contributions at KEJ. (a) natural surface emissions (wildfires plus re-emitted Hg), (b) anthropogenic emissions, (c) Hg pool, (d) regional emission and SSA processing, (e) oceanic evasion, (f) GEM re-emissions, (g) wildfires, (h) local combustion, (i) secondary sulfate. Blue line: relative contributions; red line: trendline; green text: slope of the trendline (x100% yr$^{-1}$).**

## 4 Discussion

Comparing TGM source apportionment results among the sites, natural surface emissions exceeded anthropogenic emission contributions to TGM at all three. Mean relative contributions from anthropogenic emissions were 35% at SAT and KEJ and lower at EGB. There was a clear long-term increase in the relative importance of natural surface emissions to TGM at SAT

and KEJ, which resulted from decreased anthropogenic Hg emissions and increased oceanic Hg evasion and terrestrial GEM re-emissions.

The Hg pool and subsequent long-range transport was a major source of TGM at all sites. Average relative contributions to annual TGM were 71% at KEJ, 63% at EGB, and 53% at SAT, with higher contributions from November to April. Previous source attribution analysis performed using the Global/Regional Atmospheric Heavy Metals (GRAHM) model showed that the sources of GEM in Canada mostly originated in Europe and East Asia. European sources contributed 3% of GEM at SAT, <3% at EGB, and 3.5% at KEJ via long-range transport across the Arctic. Long-range transport from East Asia had the greatest impact on GEM across Canada, contributing 16% at SAT, 14-15% at EGB, and 15% at KEJ (ECCC, 2016). The anthropogenic to natural surface emissions proportion for the Hg pool was estimated based on global Hg emissions inventory. While the percentages used in this study were consistent with some emissions inventories, i.e. ~30% for anthropogenic Hg emissions (Pirrone et al., 2010; Outridge et al., 2018; Streets et al., 2019; UNEP, 2019), this percentage is 4-6% lower in other global budgets (Shah et al., 2021; Sonke et al., 2023; Zhang et al., 2023). It is expected that the global anthropogenic to natural contributions ratio will change in the future as primary anthropogenic emissions decrease and Hg re-emissions increase.

The second most important Hg source at EGB (28%) and SAT (14%) was terrestrial surface re-emissions. Relative contributions from GEM re-emissions were greatest from May to October. GEM re-emission was only a minor source of TGM at KEJ likely because the site is in a forested area which is a net sink for GEM. The variability between sites reflects the nature of GEM surface-air exchange, which is spatially variable and dependent on factors such as solar radiation intensity, canopy shading and wetness, air and soil temperature, soil Hg content, soil moisture, soil organic matter content, vegetation and litterfall covering the soil, ambient Hg concentration, and forest uptake which is a key driver of GEM dry deposition (Zhang et al., 2009; Ottesen et al., 2013; Agnan et al., 2016; Eckley et al., 2016; Wang et al., 2016; Sommar et al., 2020). Some areas of British Columbia and Ontario have soils that are naturally enriched in Hg, which have led to higher fluxes (ECCC, 2016). Hg emissions from agricultural soils (e.g. at EGB) are greater than that of natural soils because of more frequent land disturbance which increases volatilization and soil dust resuspension (Cobbett and Van Heyst, 2007; Zhu et al., 2016). Surface re-emission is one of the least constrained processes in the Hg cycle. It can be influenced by a multitude of environmental factors, which are currently not well represented in CTMs (Zhu et al., 2016; Obrist et al., 2018). There are also limited Hg flux measurements for characterizing both spatial and temporal variations.

TGM contribution from local combustion was highest at EGB (6%) followed by SAT (4%) and KEJ (2%). These results were similar to previous GRAHM model simulations, which found Canadian sources accounted for only 3-5% of GEM near EGB, 1% near SAT, and 0.5-1% near KEJ (ECCC, 2016). Overall, the contribution by Canadian sources is typically < 1% in areas outside the vicinity of major Hg point sources according to models (ECCC, 2016). For secondary sulfate TGM contributions, the percentages ranked by site were SAT > EGB > KEJ and were under 5%.

Oceanic evasion contributed similar percentages of the TGM at SAT and KEJ (7-9.5%). As reported in global Hg budgets, oceanic Hg re-emissions are poorly constrained (Dastoor et al., 2024). A recent model simulation suggests that Hg re-

emission from oceans is underestimated by 40% (Zhang et al., 2023), whereas another study provided more modest re-emission estimates (Tang et al., 2025).

At the coastal sites, we found evidence of anthropogenic emission contributions and SSA processing. Marine transportation and shipping ports provided sources of TGM at SAT, while regional Hg emissions notably from U.S. electric utilities (fossil fuel combustion) had impacted TGM at KEJ. Because these sources also emit $SO_2$, the acidic gases formed further reacted with SSA in the MBL resulting in the formation of aged SSA. Significant reductions in both Hg and $SO_2$ emissions led to diminished impacts from anthropogenic emissions and SSA processing over time.

Wildfires affected TGM at SAT (western Canada) more than KEJ and EGB (eastern Canada). Wildfires in western Canada and the western U.S. have led to elevated $PM_{2.5}$, $O_3$, atmospheric nitrogen, and total carbon in downwind regions (Lu et al., 2016; McClure and Jaffe, 2018; Chen et al., 2019; Campbell et al., 2022; Yao and Zhang, 2024). Wildfires Hg emissions in western Canada are greater than those in eastern Canada, comprising approximately 65% of the national total wildfire Hg emissions. For the 2010-2015 period, wildfires contributed 0.2-0.4% of the daily mean GEM near SAT according to the GEM-MACH-Hg model (Fraser et al., 2018). In this study, we estimated the PMF-derived daily mean TGM contribution from wildfires to be 4.4% over the same period. For EGB, the percentage wildfire contributions to daily mean GEM/TGM were 0.4-0.8% based on the GEM-MACH-Hg model and 1.7% based on the PMF model. The corresponding percentages for KEJ were 0.3-0.5% and 2.7% of the daily mean GEM/TGM. Note that on a daily basis there can be large variability in the GEM-MACH-Hg estimated wildfire contributions with percentages up to 30% for SAT, 23% for EGB and 10% for KEJ. This variability was also seen in the PMF modeling results (Figs. 5, 10, 14). Differences in the wildfire source contributions between GEM-MACH-Hg (Fraser et al., 2018) and PMF (this study) could be due to underestimated wildfire Hg emissions in CTMs, other model parameterization uncertainties, measurement uncertainties affecting the PMF model results, FRP-approach for screening wildfire TGM contributions, etc. While model intercomparisons are common for CTMs, more comparisons conducted between CTMs and receptor models like PMF will ultimately improve source apportionment estimates for both types of air quality models. We examined wildfire impacts on gaseous Hg in this study; however, wildfires also contribute significantly to particulate Hg depending on the fuel moisture and combustion type (Obrist et al., 2008; McLagan et al., 2021). To capture the full impact of wildfires on atmospheric Hg, future source contribution analysis should include particulate Hg measurements if possible.

## 5 Conclusions

Source contributions to three rural-remote TGM sites were estimated using the PMF model. We examined long-term trends in TGM source contributions to understand the major drivers of the observed TGM trends, as well as analyzed the variability in interannual, seasonal and daily TGM contributions. Anthropogenic sources that were inferred from PMF include local combustion, secondary sulfate, and the anthropogenic portion of the Hg pool (~31%). Additionally, shipping emissions were

identified at SAT, and regional emissions from the U.S. northeast were identified at KEJ. Natural surface emission contributions comprised terrestrial GEM re-emissions, oceanic Hg evasion, wildfires, and the proportion of the Hg pool from natural surface emissions (~69%). Additional TGM contributions from crustal/soil dust and road salt were found at EGB. At SAT, the decreasing TGM trend was attributed to decreasing shipping and GEM re-emissions. The long-term decreasing TGM trend at EGB was attributed to decreasing Hg pool contributions, though other local sources contributed to the initial decline in TGM and the flat trend after 2013. The long-term TGM trend at KEJ was driven by the Hg pool, regional emissions, and GEM re-emissions. When analyzing on a shorter timescale, Hg emissions from electric utilities and oil and gas pipelines and storage had a strong influence on TGM. Overall, emission contributions from natural surfaces (wildfires plus re-emitted Hg) were greater than anthropogenic contributions to annual TGM at all sites.

In the last decade, the downward trend in anthropogenic emission contributions led to increasing Hg contributions from natural surfaces. The latter can potentially be accelerated by global warming as this can drive up terrestrial and oceanic Hg re-emissions and wildfire Hg emissions. These emissions not only contribute to downwind areas, but also to the global Hg pool, which in the case of GEM impacts other regions through long-range transport. Hg emissions from natural surfaces are overall less constrained compared with combustion sources, and they make up the bulk of the global Hg emissions. It is important to increase monitoring of terrestrial and oceanic surface re-emissions, track their long-term trends, and examine how climate perturbations are affecting the emissions and Hg cycling in the environment.

**Data availability:** All datasets used in this study are publicly available (Table S1).

**Author contribution:** I.C.: conceptualization, methodology, formal analysis, validation, writing – original draft, review & editing. A.C.: supervision, validation, writing – review & editing. L.Z.: conceptualization, methodology, writing – review & editing. A.S.: validation, writing – review & editing.

**Competing interests:** One of the authors is a member of the editorial board of Atmospheric Chemistry and Physics.

**Acknowledgements:** We acknowledge ECCC Canadian Air and Precipitation Monitoring Network (CAPMoN), National Air Pollution Surveillance (NAPS) program, Canadian Greenhouse Gas Measurement program, Climate Data Services; USEPA Air Quality System; Interagency Monitoring of Protected Visual Environments (IMPROVE); and NASA/MODIS for the provision of datasets used in this publication. Special thanks to CAPMoN and National Atmospheric Chemistry (NAtChem) teams; Amy Hou for data extraction/processing; Doug Worthy for Egbert CO data; Anne Marie Macdonald, James Kuchta and Kenny Yan for internal review.

## References

Agnan, Y., Le Dantec, T., Moore, C. W., Edwards, G. C., and Obrist, D.: New constraints on terrestrial surface–atmosphere fluxes of gaseous elemental mercury using a global database, Environ. Sci. Technol., 50(2), 507-524, 2016.

Anastasopolos, A.T., Sofowote, U.M., Hopke, P.K., Rouleau, M., Shin, T., Dheri, A., Peng, H., Kulka, R., Gibson, M.D., Farah, P.M. and Sundar, N.: Air quality in Canadian port cities after regulation of low-sulphur marine fuel in the North American Emissions Control Area, Sci. Total Environ., 791, 147949, 2021.

Brown, S.G., Eberly, S., Paatero, P. and Norris, G.A.: Methods for Estimating Uncertainty in PMF Solutions: Examples with Ambient Air and Water Quality Data and Guidance on Reporting PMF Results, Sci. Total Environ., 518, 626-635, 2015.

Campbell, P.C., Tong, D., Saylor, R., Li, Y., Ma, S., Zhang, X., Kondragunta, S. and Li, F.: Pronounced increases in nitrogen emissions and deposition due to the historic 2020 wildfires in the western US, Sci. Total Environ., 839, 156130, 2022.

Chen, J., Anderson, K., Pavlovic, R., Moran, M.D., Englefield, P., Thompson, D.K., Munoz-Alpizar, R. and Landry, H.: The FireWork v2. 0 air quality forecast system with biomass burning emissions from the Canadian Forest Fire Emissions Prediction System v2. 03, Geosci. Model Dev., 12(7), 3283-3310, 2019.

Cheng I., Xu X., and Zhang L.: Overview of receptor-based source apportionment studies for speciated atmospheric mercury. Atmos. Chem. Phys., 15, 7877–7895, 2015.

Cheng, I., Zhang, L., Castro, M. and Mao, H.: Identifying Changes in Source Regions Impacting Speciated Atmospheric Mercury at a Rural Site in the Eastern United States, J. Atmos. Sci., 74(9), 2937-2947, 2017.

Cobbett, F. D., and Van Heyst, B. J.: Measurements of GEM fluxes and atmospheric mercury concentrations (GEM, RGM and Hgp) from an agricultural field amended with biosolids in Southern Ont., Canada (October 2004–November 2004), Atmos. Environ., 41(11), 2270-2282, 2007.

Cole, A. S., Steffen, A., Eckley, C. S., Narayan, J., Pilote, M., Tordon, R., Graydon, J. A., St. Louis, V.L., Xu, X. and Branfireun, B. A.: A survey of mercury in air and precipitation across Canada: patterns and trends, Atmosphere, 5(3), 635-668, 2014.

Custodio, D., Ebinghaus, R., Spain, T. G., and Bieser, J.: Source apportionment of atmospheric mercury in the remote marine atmosphere: Mace Head GAW station, Irish western coast, Atmos. Chem. Phys., 20(13), 7929-7939, 2020.

Dastoor, A., Angot, H., Bieser, J., Brocza, F., Edwards, B., Feinberg, A., Feng, X., Geyman, B., Gournia, C., He, Y., Hedgecock, I. M., Ilyin, I., Keating, T., Kirk, J., Lin, C.-J., Lehnherr, I., Mason, R., McLagan, D., Muntean, M., Rafaj, P., Roy, E. M., Ryjkov, A., Selin, N. E., De Simone, F., Soerensen, A. L., Steenhuisen, F., Travnikov, O., Wang, S., Wang, X., Wilson, S., Wu, R., Wu, Q., Zhang, Y., Zhou, J., Zhu, W., and Zolkos, S.: The Multi-Compartment Hg Modeling and Analysis Project (MCHgMAP): Mercury modeling to support international environmental policy. Geosci. Model Dev. Discuss. [preprint], https://doi.org/10.5194/gmd-2024-65, in review, 2024.

Dastoor, A., Ryjkov, A., Kos, G., Zhang, J., Kirk, J., Parsons, M., and Steffen, A.: Impact of Athabasca oil sands operations on mercury levels in air and deposition, Atmos. Chem. Phys., 21(16), 12783-12807, 2021.

Dastoor, A., Wilson, S.J., Travnikov, O., Ryjkov, A., Angot, H., Christensen, J.H., Steenhuisen, F. and Muntean, M.: Arctic atmospheric mercury: Sources and changes, Sci. Total Environ., 839, 156213, 2022.

Driscoll, C. T.; Mason, R. P.; Chan, H. M.; Jacob, D. J.; Pirrone, N.: Mercury as a Global Pollutant: Sources, Pathways, and Effects, Environ. Sci. Technol., 47, (10), 4967-4983, 2013.

Eckley, C.S., Parsons, M.T., Mintz, R., Lapalme, M., Mazur, M., Tordon, R., Elleman, R., Graydon, J.A., Blanchard, P. and St. Louis, V.: Impact of closing Canada's largest point-source of mercury emissions on local atmospheric mercury concentrations, Environ. Sci. Technol., 47(18), 10339-10348, 2013.

Eckley, C.S., Tate, M.T., Lin, C.J., Gustin, M., Dent, S., Eagles-Smith, C., Lutz, M.A., Wickland, K.P., Wang, B., Gray, J.E., Edwards, G.C., Krabbenhoft, D. P., and Smith, D. B.: Surface-air mercury fluxes across Western North America: A synthesis of spatial trends and controlling variables, Sci. Total Environ., 568, 651-665, 2016.

Environment and Climate Change Canada (ECCC): 2004 Canadian Acid Deposition Science Assessment, Meteorological Services of Canada, http://www.publications.gc.ca/pub?id=9.688243&sl=0, 2004.

Environment and Climate Change Canada (ECCC):, Canadian mercury science assessment: report. Gatineau, Quebec. ISBN 978-0-660-04499-6. www.publications.gc.ca/pub?id=9.810484&sl=0, 2016.

Feinberg, A., Dlamini, T., Jiskra, M., Shah, V., and Selin, N. E.: Evaluating atmospheric mercury (Hg) uptake by vegetation in a chemistry-transport model, Environ. Sci. Process. Impacts, *24*(9), 1303-1318, 2022.

Fisher, J. A., Jacob, D. J., Soerensen, A. L., Amos, H. M., Steffen, A., and Sunderland, E. M.: Riverine source of Arctic Ocean mercury inferred from atmospheric observations, Nat. Geosci., *5*(7), 499-504, 2012.

Fraser, A., Dastoor, A., and Ryjkov, A.: How important is biomass burning in Canada to mercury contamination?, Atmos. Chem. Phys., 18(10), 7263-7286, 2018.

Gratz, L. E., and Keeler, G. J.: Sources of mercury in precipitation to Underhill, VT, Atmos. Environ., 45(31), 5440-5449, 2011.

Government of British Columbia (B.C.): Statistics & Geospatial Data, Wildfire Averages, https://www2.gov.bc.ca/gov/content/safety/wildfire-status/about-bcws/wildfire-statistics/wildfire-averages, 2025.

Holmes, C. D., Jacob, D. J., Mason, R. P., and Jaffe, D. A.: Sources and deposition of reactive gaseous mercury in the marine atmosphere, Atmos. Environ., 43(14), 2278-2285, 2009.

Hong, Y. S., Kim, Y. M. and Lee, K. E.: Methylmercury exposure and health effects. Journal of preventive medicine and public health, 45(6), 353-363, 2012.

Horowitz, H. M., Jacob, D. J., Zhang, Y., Dibble, T. S., Slemr, F., Amos, H. M., Schmidt, J. A., Corbitt, E. S., Marais, E. A., and Sunderland, E. M.: A new mechanism for atmospheric mercury redox chemistry: implications for the global mercury budget, Atmos. Chem. Phys., 17, 6353–6371, 2017.

Huang, J., Choi, H. D., Hopke, P. K., and Holsen, T. M.: Ambient mercury sources in Rochester, NY: results from principle components analysis (PCA) of mercury monitoring network data, Environ. Sci. Technol., 44(22), 8441-8445, 2010.

Jeffery, P. S., Drummond, J. R., Zou, J., and Walker, K. A.: Identifying episodic carbon monoxide emission events in the MOPITT measurement dataset, Atmos. Chem. Phys., 24, 4253–4263, https://doi.org/10.5194/acp-24-4253-2024, 2024.

Keeler, G. J., Landis, M. S., Norris, G. A., Christianson, E. M., and Dvonch, J. T.: Sources of mercury wet deposition in eastern Ohio, USA, Environ. Sci. Technol., 40(19), 5874-5881, 2006.

Lee, E. J., Kenkel, N., and Booth, T.: Atmospheric deposition of macronutrients by pollen in the boreal forest, Ecosci., 3(3), 304-309, 1996.

Li, C., Sonke, J.E., Le Roux, G., Piotrowska, N., Van der Putten, N., Roberts, S.J., Daley, T., Rice, E., Gehrels, R., Enrico, M., Mauquoy, D., Roland, T. P., and De Vleeschouwer, F.: Unequal anthropogenic enrichment of mercury in earth's northern and southern hemispheres, ACS Earth Space Chem., *4*(11), 2073-2081, 2020.

Liu, W., Hopke, P. K., Han, Y. J., Yi, S. M., Holsen, T. M., Cybart, S., Kozlowski, K., and Milligan, M.: Application of receptor modeling to atmospheric constituents at Potsdam and Stockton, NY, Atmos. Environ., 37(36), 4997-5007, 2003.

Lu, X., Zhang, L., Yue, X., Zhang, J., Jaffe, D.A., Stohl, A., Zhao, Y. and Shao, J.: Wildfire influences on the variability and trend of summer surface ozone in the mountainous western United States, Atmos. Chem. Phys., 16(22), 14687-14702, 2016.

MacSween, K., Stupple, G., Aas, W., Kyllönen, K., Pfaffhuber, K.A., Skov, H., Steffen, A., Berg, T., and Mastromonaco, M.N.: Updated trends for atmospheric mercury in the Arctic: 1995–2018, Sci. Total Environ., 837, 155802, 2022.

Mazur, M., Mintz, R., Lapalme, M., and Wiens, B.: Ambient air total gaseous mercury concentrations in the vicinity of coal-fired power plants in Alberta, Canada, Sci. Total Environ., 408(2), 373-381, 2009.

McClure, C. D., and Jaffe, D. A.: US particulate matter air quality improves except in wildfire-prone areas, Proc. Natl. Acad. Sci., 115(31), 7901-7906, 2018.

McLagan, D. S., Stupple, G. W., Darlington, A., Hayden, K., and Steffen, A.: Where there is smoke there is mercury: Assessing boreal forest fire mercury emissions using aircraft and highlighting uncertainties associated with upscaling emissions estimates, Atmos. Chem. Phys., 21(7), 5635-5653, 2021.

Michael, R., Stuart, A. L., Trotz, M. A., and Akiwumi, F.: Source apportionment of wet-deposited atmospheric mercury in Tampa, Florida. Atmos. Res., 170, 168-175, 2016.

NASA Near Real-Time and MODIS Active Fire Detections (TXT/CSV format). Dataset. Accessed 1 October 2023.

Norris, G., Duvall, R., Brown, S., and Bai, S.: EPA Positive Matrix Factorization (PMF) 5.0 Fundamentals and User Guide. Office of Research and Development, Washington, DC 20460. https://www.epa.gov/air-research/epa-positive-matrix-factorization-50-fundamentals-and-user-guide, 2014.

Obrist, D., Kirk, J. L., Zhang, L., Sunderland, E. M., Jiskra, M., and Selin, N. E.: A review of global environmental mercury processes in response to human and natural perturbations: Changes of emissions, climate, and land use, Ambio, 47(2), 116-140, 2018.

Obrist, D., Moosmüller, H., Schürmann, R., Chen, L. W. A., and Kreidenweis, S. M.: Particulate-phase and gaseous elemental mercury emissions during biomass combustion: controlling factors and correlation with particulate matter emissions, Environ. Sci. Technol., 42(3), 721-727, 2008.

Ottesen, R.T., Birke, M., Finne, T.E., Gosar, M., Locutura, J., Reimann, C., Tarvainen, T. and GEMAS Project Team: Mercury in European agricultural and grazing land soils, Appl. Geochem., 33, 1-12, 2013.

Outridge, P. M., Mason, R. P., Wang, F., Guerrero, S., and Heimburger-Boavida, L. E.: Updated global and oceanic mercury budgets for the United Nations Global Mercury Assessment 2018, Environ. Sci. Technol., 52(20), 11466-11477, 2018.

Pancras, J. P., Landis, M. S., Norris, G. A., Vedantham, R., and Dvonch, J. T.: Source apportionment of ambient fine particulate matter in Dearborn, Michigan, using hourly resolved PM chemical composition data, Sci. Total Environ., 448, 2-13, 2013.

Pirrone, N., Cinnirella, S., Feng, X., Finkelman, R.B., Friedli, H.R., Leaner, J., Mason, R., Mukherjee, A.B., Stracher, G.B., Streets, D.G. and Telmer, K.: Global mercury emissions to the atmosphere from anthropogenic and natural sources. Atmos. Chem. Phys., 10(13), 5951-5964, 2010.

Qin, X., Zhang, L., Wang, G., Wang, X., Fu, Q., Xu, J., Li, H., Chen, J., Zhao, Q., Lin, Y. and Huo, J.: Assessing contributions of natural surface and anthropogenic emissions to atmospheric mercury in a fast-developing region of eastern China from 2015 to 2018, Atmos. Chem. Phys., 20(18), 10985-10996, 2020.

Rutter, A. P., and Schauer, J. J.: The impact of aerosol composition on the particle to gas partitioning of reactive mercury. Environ. Sci. Technol., 41(11), 3934-3939, 2007.

Selin, N. E., and Jacob, D. J.: Seasonal and spatial patterns of mercury wet deposition in the United States: Constraints on the contribution from North American anthropogenic sources, Atmos. Environ., 42(21), 5193-5204, 2008.

Shah, V., Jacob, D. J., Thackray, C. P., Wang, X., Sunderland, E. M., Dibble, T. S., Saiz-Lopez, A., Černušák, I., Kellö, V., Castro, P. J., Wu, R., and Wang, C.: Improved mechanistic model of the atmospheric redox chemistry of mercury, Environ. Sci. Technol., *55*(21), 14445-14456, 2021.

Shah, V., Jaeglé, L., Gratz, L.E., Ambrose, J.L., Jaffe, D.A., Selin, N.E., Song, S., Campos, T.L., Flocke, F.M., Reeves, M. and Stechman, D.: Origin of oxidized mercury in the summertime free troposphere over the southeastern US, Atmos. Chem. Phys., *16*(3), 1511-1530, 2016.

Sommar, J., Osterwalder, S., and Zhu, W.: Recent advances in understanding and measurement of Hg in the environment: Surface-atmosphere exchange of gaseous elemental mercury (Hg0), Sci. Total Environ., 721, 137648, 2020.

Sonke, J. E., Angot, H., Zhang, Y., Poulain, A., Björn, E., and Schartup, A., 2023. Global change effects on biogeochemical mercury cycling, Ambio, *52*(5), 853-876, 2023.

Streets, D. G., Horowitz, H. M., Lu, Z., Levin, L., Thackray, C. P., and Sunderland, E. M.: Global and regional trends in mercury emissions and concentrations, 2010–2015, Atmos. Environ., 201, 417-427, 2019.

Tang, K., Song, Z., Fu, X., Zhang, Y., Zhang, H., Sun, Y., Zhang, H., Wu, X., Deng, Q., Zhang, L., Suratman, S., Seng, T. H., and Feng, X. : An Interhemispheric Difference in Atmospheric Gaseous Elemental Mercury Isotopes Reveals a New Insight in Oceanic Mercury Emissions, J. Geophys. Res., e2024JD042178, 2025.

UN Environment (UNEP): Global Mercury Assessment 2018. UN Environment Programme, Chemicals and Health Branch Geneva, Switzerland. https://www.unep.org/resources/publication/global-mercury-assessment-2018, 2019.

Wang, X., Lin, C. J., Yuan, W., Sommar, J., Zhu, W., and Feng, X.: Emission-dominated gas exchange of elemental mercury vapor over natural surfaces in China, Atmos. Chem. Phys., 16(17), 11125-11143, 2016.

Wang, Y., Huang, J., Hopke, P. K., Rattigan, O. V., Chalupa, D. C., Utell, M. J., and Holsen, T. M., 2013. Effect of the shutdown of a large coal-fired power plant on ambient mercury species, Chemosphere, 92(4), 360-367.

Yao, X. and Zhang, L.: Identifying decade trends in deweathered concentrations of criteria air pollutants in Canadian urban atmospheres with machine learning approaches, Atmos. Chem. Phys., 24, 7773-7791, 2024.

Yu, J., Yan, C., Liu, Y., Li, X., Zhou, T., and Zheng, M.: Potassium: a tracer for biomass burning in Beijing?, Aerosol Air Qual. Res., 18(9), 2447-2459, 2018.

Zhang, L., Vet, R., Wiebe, A., Mihele, C., Sukloff, B., Chan, E., Moran, M. D., and Iqbal, S.: Characterization of the size-segregated water-soluble inorganic ions at eight Canadian rural sites, Atmos. Chem. Phys., 8, 7133–7151, https://doi.org/10.5194/acp-8-7133-2008, 2008.

Zhang, L., Wright, L. P., and Blanchard, P.: A review of current knowledge concerning dry deposition of atmospheric mercury, Atmos. Environ., 43(37), 5853-5864, 2009.

Zhang, Y., Jacob, D.J., Horowitz, H.M., Chen, L., Amos, H.M., Krabbenhoft, D.P., Slemr, F., St. Louis, V.L. and Sunderland, E.M.: Observed decrease in atmospheric mercury explained by global decline in anthropogenic emissions, Proc. Natl. Acad. Sci., *113*(3), 526-531, 2016.

Zhang, Y., Zhang, P., Song, Z., Huang, S., Yuan, T., Wu, P., Shah, V., Liu, M., Chen, L., Wang, X., Zhou, J., and Agnan, Y.: An updated global mercury budget from a coupled atmosphere-land-ocean model: 40% more re-emissions buffer the effect of primary emission reductions, One Earth, 6(3), 316-325, 2023.

Zhou, J., Obrist, D., Dastoor, A., Jiskra, M., and Ryjkov, A.: Vegetation uptake of mercury and impacts on global cycling, Nature Reviews Earth and Environ., *2*(4), 269-284, 2021.

Zhu, W., Lin, C. J., Wang, X., Sommar, J., Fu, X., and Feng, X.: Global observations and modeling of atmosphere–surface exchange of elemental mercury: a critical review, Atmos. Chem. Phys., 16(7), 4451-4480, 2016.